

Design of New Ecofriendly Schiff Base Inhibitors for Carbon Steel Corrosion Protection in Acidic Solutions: Electrochemical, Surface, and Theoretical Studies

Qahtan A. Yousif,* Ahmed Abdel Nazeer,* Zainb Fadel, Latifa A. Al-Hajji, and Kamal Shalabi



Cite This: *ACS Omega* 2024, 9, 14153–14173



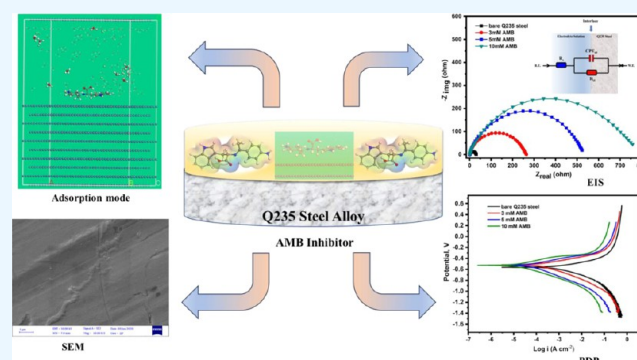
Read Online

ACCESS |

Metrics & More

Article Recommendations

ABSTRACT: Corrosion poses a significant problem for several industrial sectors, inducing continuous research and development of corrosion inhibitors for use across a wide range of industrial applications. Here, we report the effectiveness of three newly developed Schiff bases derived from amino acids and 4-aminoacetophenone, namely, **AIP**, **AMB**, and **AlmP**, as environmentally friendly corrosion inhibitors for Q235 steel in hydrochloric acid using electrochemical and surface analyses, in addition to theoretical techniques. The electrochemical findings of potentiodynamic polarization (PDP) demonstrated that the explored compounds serve as mixed-type inhibitors and can effectively suppress steel corrosion, with maximal protection efficiencies of 93.15, 96.01, and 77.03% in the presence of **AIP**, **AMB**, and **AlmP**, respectively, at a concentration of 10 mM. The electrochemical impedance spectroscopy (EIS) and polarization results confirmed the growth of a durable protective barrier on the steel surface in the existence of the inhibitors, which is responsible for decreasing the metallic dissolution. Results were further supported by scanning electron microscopy (SEM), energy-dispersive X-ray spectroscopy (EDS), UV–vis, and Fourier transform infrared (FTIR), which ascribed the development of inhibitor–adsorption films on the steel surface. The results of EDS and XPS analyses demonstrated the existence of the distinctive elements of the inhibitors on the metallic surface. Furthermore, density functional theory (DFT) calculations and Monte Carlo (MC) simulations showed the electronic structure of the examined inhibitors and their optimized adsorption configurations on the steel surface, which helped in explaining the anticorrosion mechanism. Finally, the theoretical and experimental findings exhibit a high degree of consistency.



1. INTRODUCTION

Corrosion affects the vast majority of manufacturing industries and can have annual costs in the billions of dollars. Acids and bases are frequently encountered in industrial processes because of their proximity to these environments.¹ They have a damaging effect on the environment. On the other hand, acids play a crucial role in the industrial sector, particularly in the cleaning systems used in the food industry, industrial cleaning, acid scaling, refining crude oil, acid pickling, and petrochemical processes.² In factories, acid treatments are often used to eliminate rust and scale. Steel and other metal types are often cleaned with hydrochloric acid. Most of the time, inhibitors are frequently used in these procedures to regulate how much metal dissolves. Economic, safety, and environmental concerns all point to improved methods for preventing metal corrosion.³ Strategies that try to quench, delay, and halt anodic, cathodic, or both processes can help reduce it. Metal corrosion can be significantly reduced by applying several strategies, such as material modernization, alloying, environmental cleansing, various coatings, and inhibitors.⁴ Corrosion inhibitors must be

used to protect underlying materials from corrosion by providing adsorption and excellent anticorrosive properties.⁵ Inhibitors are commonly utilized in these procedures to regulate metal solubility.⁶ Acid corrosion inhibitors typically comprise organic molecules' nitrogen, sulfur, and oxygen atoms. Organic compounds rich in nitrogen have long been recognized as effective corrosion inhibitors in dilute hydrochloric acid solutions.⁷ Corrosion inhibitors, like heterocycle compounds, slow the corrosion process when applied to a corrosive medium in small amounts; they are considered an effective and cost-efficient technique. Many recent studies have used this strategy to develop corrosion control methods.⁸ An inhibitor's effectiveness depends on several elements, such as its solubility,

Received: December 4, 2023

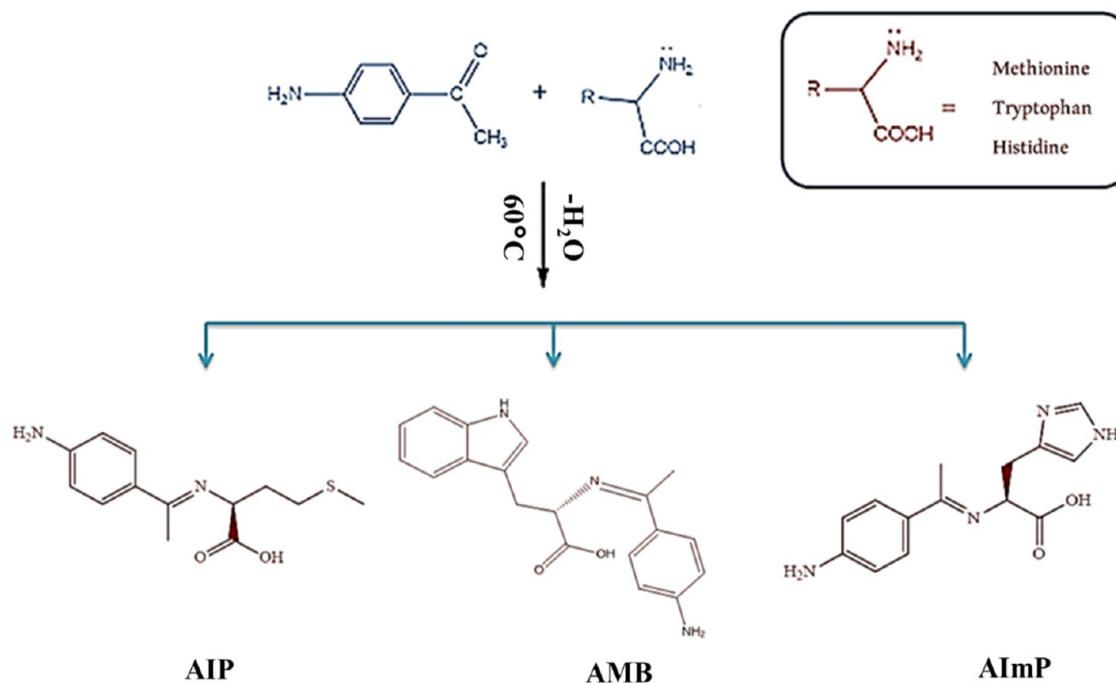
Revised: February 26, 2024

Accepted: February 29, 2024

Published: March 18, 2024



Scheme 1. Scheme for Preparation of Schiff Base Derivatives AIP, AMB, and AImP



reaction to the corrosive medium, and effective centers that can interact with the metallic surface. Because of their abundance of active regions, functional groups, and π -electrons, aromatic heterocyclics are among the most frequently employed materials as anticorrosion compounds.⁹ This is because they readily interact with the metallic surface forming a protective barrier through chemical adsorption, physical adsorption, or both.¹⁰

Schiff bases have gained attraction as corrosion inhibitors due to their superior adsorption and film-forming capabilities. The coordination of the imine group with the ions on the metallic surface is responsible for this strong behavior. Generally, Schiff bases are created from low-cost precursors by combining an aldehyde or ketone with the condensation- NH_2 moiety.¹¹ In addition, Schiff bases derived from amino acids have attracted the attention of researchers owing to their use in numerous pharmacological applications and other fields.^{12–14} Furthermore, they are considered suitable anticorrosion materials due to their efficacy against corrosion problems in multiple environments. The relationship among the molecular structure of these derivatives and their protection efficiency is strong.¹⁵ In their planar structures, N and S atoms contain electron pairs.¹⁶ Due to the presence of π -electrons in their chemical structures, these inhibitors readily adsorb on the metal surface.¹⁷ Temperatures and the acidity of a solution, among others, influence the corrosion rate of carbon steel; along with numerous industrial and environmental factors, these factors strongly correlate with the economic costs of various manufacturing disciplines. Therefore, researchers have increased their efforts to discover effective strategies to mitigate the corrosion of these facilities, particularly oil factories that are susceptible to these conditions due to their work. Anticorrosion chemicals are harmful,¹⁸ so chemists produce corrosive inhibitors with no toxic units and high inhibitory efficiency. Thus, biodegradable and nontoxic inhibitors are increasingly important. Schiff bases derived from amino acids were extensively recognized as green corrosion inhibitors mainly owing to their nontoxic nature and biodegradable character-

istics. There have been many studies on the use of Schiff bases as corrosion inhibitors.^{19–22} The outstanding performance of amino acid derivatives as anticorrosion agents in various media motivates our laboratory team to seek the materials with the highest inhibition efficiencies to supplement our previous research in this field. In this context, the current study details the synthesis of three Schiff bases derived from amino acids and 4-aminoacetophenone, namely, (*S,E*)-2-(1-(4-aminophenyl)ethylideneamino)-4-(methylthio)butanoic acid (**AIP**), (*S,Z*)-2-((1-(4-aminophenyl)ethylideneamino)-3-(1*H*-indol-3-yl)propanoic acid (**AMB**), and (*S*)-2-((1-(4-aminophenyl)ethylideneamino)-3-(1*H*-imidazol-4-yl)propanoic acid (**AImP**). Synthesized **AIP**, **AMB**, and **AImP** inhibitors have lone pair electrons with nitrogen, oxygen, and sulfur and unsaturated π -electrons and carbon chains (producing a hydrophobic effect). This meets the requirements for a compound to bind to the surface of steel and suppress corrosion. Electrochemical measurement techniques were used to study and test the prepared compounds' ability to inhibit the carbon steel corrosion used to make Iraqi oil tanks. Several spectroscopic methods were used to confirm the electrochemical results. These included scanning electron microscopy (SEM), energy-dispersive X-ray spectroscopy (EDS), ultraviolet–visible (UV–vis) spectroscopy, X-ray photoelectron spectroscopy (XPS), and Fourier transform infrared (FTIR) spectroscopy. Also, density functional theory (DFT) and Monte Carlo (MC) simulations were conducted to delve deeper into corrosion protection mechanisms.

2. EXPERIMENTAL TECHNIQUES

2.1. Synthesis of 4-Aminoacetophenone and Amino Acid Derivative Inhibitors.

1 mmol of 4-aminoacetophenone was dissolved in 10 mL of methanol solvent, with continuous stirring until complete dissolution; then, two drops of glacial acetic acid was added as a catalyst. Then, 1 mmol of the amino acids (methionine, tryptophan, and histidine) was dissolved in 15 mL of methanol solvent. The amino acid solution was added

slowly to the aromatic ketone, and the mixture was refluxed for 8–10 h at a temperature of 60 °C in a water bath. All products were washed, dried, and recrystallized. The product's amino acid derivatives were solid powders. Thin-layer chromatography followed the reaction using the mobile phase at 4:1 ethyl alcohol to benzene. Scheme 1 shows the preparation scheme for synthesized Schiff base derivatives.

2.2. Electrodes and Electrolytes. The dimensions of the Q235 steel sample used in the electrochemical measurements were $1 \times 1 \times 0.5 \text{ cm}^2$, with a total surface area of 1 cm^2 . The composition was C = 0.174, Mn = 1.361, Si = 0.367, S = 0.003, P = 0.0116, Ni = 0.033, Cu = 0.012, and Fe = 98.037 by weight. For removing the undesirable layer from the steel specimen's surface, grades of emery paper ranging from 80 to 2000 were utilized for cleansing and polishing. Then, demineralized purified water and acetone were utilized for washing followed by dehydrating the samples before the test. The necessary hydrochloric acid solution with a concentration of 1.0 M was made by diluting concentrated HCl with demineralized pure H₂O. Merck supplied concentrated hydrochloric acid (37%). Subsequently, multiple molar concentrations of each amino acid derivative were prepared by using diluted hydrochloric acid at a concentration of 1.0 M. The molecular weight of each amino acid derivative determined these concentrations. The studied Schiff base derivatives have exhibited excellent solubility in acidic water after dissolving in a very little amount of ethanol. Moreover, because the chosen corrosive electrolyte undergoes a process of spontaneous corrosion, no external stimulation or shaking is required for the process to progress.

2.3. Electrochemical Technique. A Q235 steel electrode with a cm^2 active surface area is used in an electrochemical cell. An epoxy holder supported the Q235 steel sample as a working electrode (WE). It employed a saturated calomel electrode (SCE) as the reference electrode and used platinum metal for the counter electrode (CE). Various concentrations of the explored compounds in the acidic electrolyte were applied to the working electrode in a volume of 200 mL. The Gamry framework software (version 7.10) was used to acquire data from the potentiostat, galvanostat, and ZRA analyzer used in electrochemical analysis. Gamry Echem Analyst (version 6.23) was used to determine the output data's fitting and graphing. Before conducting every electrochemical test, the Q235 steel electrode was immersed in an acid electrolyte for 1800 s to attain a stable, steady state for the open circuit potential (OCP). The potential values for potentiodynamic polarization (PDP) ranged from -0.4 to 0.6 V at a scan rate of 0.2 mV s^{-1} at 25 °C. In addition, the amended values for electrochemical impedance spectroscopy (EIS) were extremely small voltage ($\pm 10 \text{ mV}$) with a frequency range of 1 Hz to 100 kHz and 10 points per decade at 25 °C.

2.4. UV–Visible, FTIR, XPS, SEM, and EDS Mapping Spectral Surface Analyses. The complex formation among the explored amino acid derivatives and Q235 steel cations was demonstrated by monitoring the variations in wavelength values after 48 h of exposure to a corrosive media at an ambient temperature (using a UV–vis spectrophotometer; specifically, a double-beam UV–vis spectrophotometer, 190–1100 nm, Shimadzu brand). In addition, the FTIR (Bruker brand at a range of $400\text{--}4000 \text{ cm}^{-1}$) technique was used to analyze the inhibitors and the film produced on the Q235 steel surface after immersion in a 1.0 M HCl solution including the inhibitors to illustrate the adsorption process of the examined compounds under study (AIP, AMB, and AIMP). XPS test was performed

by an ESCA LAB 250Xi (Thermo Scientific, U.K.). Al K α radiation (1486.6 eV) with a spot size of $850 \mu\text{m}$ was used as the X-ray irradiation source. The spectral acquisitions were collected and deconvoluted with Avantage software, version v5.956. SEM and EDS mapping capabilities (JEOL, IT200 SEM) were utilized for surface morphological examination. Coupons of Q235 steel with dimensions of $2 \text{ cm} \times 2 \text{ cm} \times 0.5 \text{ cm}$ were abraded and cleansed with abrasive paper, with grades ranging from 1000 to 2000 prior to being exposed to the corrosive media for 24 h and subsequent examination. Before the investigation, the Q235 steel samples were washed with demineralized H₂O and dehydrated after 24 h. The steel coupons were affixed to the sample holder, and SEM testing was conducted at high magnification to acquire an excellently detailed image of the Q235 sample under examination. A mapping-enhanced EDS was operated to determine the organic elements adsorbed to the surface of the steel. This was done to show that the complexation of the synthesized derivatives and Q235 steel cations protects the surface.

2.5. Theoretical Computations. DFT calculations executed via B₃LYP-functional with the DNP 4.4 basis set in the Dmol³ module of BIOVIA Materials Studio 2017 software were applied to investigate the energy minimization of AIP, AMB, and AIMP molecules in aqueous conditions.²³ The DFT parameters, involving E_{HOMO} , E_{LUMO} , the energy gap (ΔE), electronegativity (χ), hardness (η), global softness (σ), electrophilicity index (ω) and the number of electrons transported (ΔN), $\Delta E_{\text{back-donation}}$, and dipole moment (μ), have been calculated using the following formulas²⁴

$$\chi = \frac{-E_{\text{HOMO}} - E_{\text{LUMO}}}{2} \quad (1)$$

$$\eta = \frac{1}{\sigma} = \frac{E_{\text{LUMO}} - E_{\text{HOMO}}}{2} \quad (2)$$

$$\Delta N = \frac{\phi - \chi_{\text{inh}}}{2(\eta_{\text{Fe}} - \eta_{\text{inh}})} \quad (3)$$

$$\Delta E_{\text{back-donation}} = \frac{-\eta}{4} \quad (4)$$

where ϕ is the work function of Fe(110), χ_{inh} is the inhibitor electronegativity, η_{Fe} is the hardness of Fe (0 eV), and η_{inh} is the chemical hardness of the inhibitor.

For MC simulations, the adsorption locator module in BIOVIA Materials Studio 2017 software was utilized to discover the optimum adsorption arrangements of the AIP, AMB, and AIMP on the Fe(110) surface.²⁵ The optimization of the adsorbate molecules was performed using the COMPASS force field.²⁶ Then, in a simulation box ($37.24 \text{ \AA} \times 37.24 \text{ \AA} \times 59.81 \text{ \AA}$), the adsorption of the investigated compounds, chloride ions, hydronium ions, and H₂O molecules on the Fe(110) surface was accomplished.²⁷

3. RESULTS AND DISCUSSION

3.1. Confirmation of Amino Acid Derivative Synthesis.

The physicochemical parameters of the AIP, AMB, and AIMP have been determined, including color, melting point, and elemental percentages. The resulting AIP compound is a light brown powder that is a solid. With a melting point of 205–207 °C, the yield was 73%. The AMB and AIMP yield and melting point values were 64% (200–202 °C) and 85% (204–206 °C), respectively. The brown powder represented the AMB

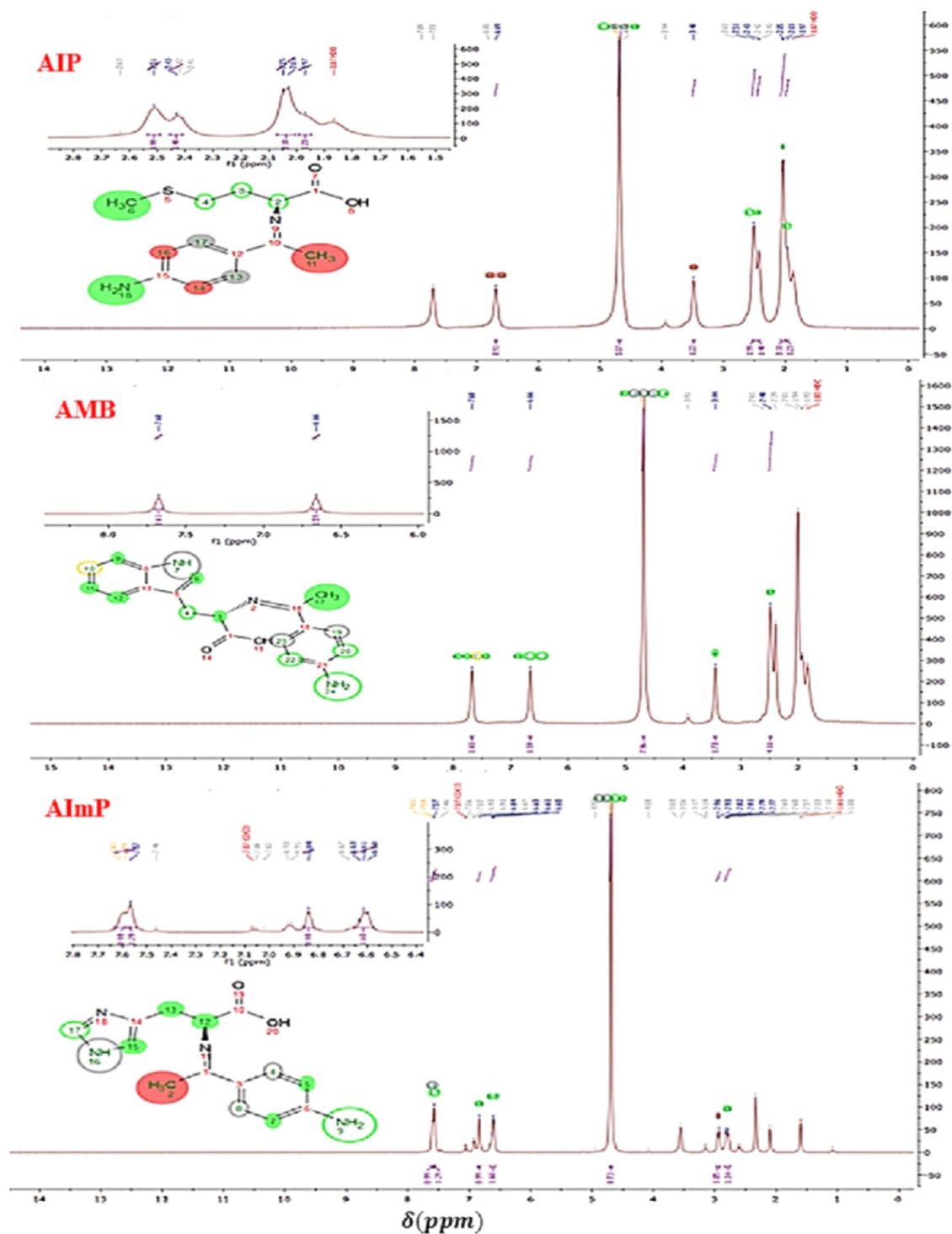


Figure 1. ^1H NMR spectra of AIP, AMB, and AImP.

component, whereas the yellow powder represented the AImP derivative. It is worth noting that ^1H and ^{13}C NMR investigations revealed the molecular structures of AIP, AMB, and AImP. The ^1H and ^{13}C NMR spectra are depicted in Figures 1 and 2, respectively. The ^1H NMR (D_2O) spectra of AIP, AMB, and AImP revealed distinct signals (Figure 1) at $\delta(\text{ppm}) = 1.9$ (s, C–H3 aliphatic), 2 (s, C–H6 aliphatic), 2.4 (m, C–H3, 14 aliphatic), 3.4 (m, C–H11 aliphatic), 6.7 (m, C–H14, 16 aromatic), and 4.7 (m, C–H17, 18, 13, 2 aromatic) for AIP. The $\delta(\text{ppm})$ values for the AMB are 2.5 (s, C–H17 aliphatic), 4.7 (d,

C–H24, 23, 19, 7, 3 aliphatic), 7.6 (m, C–H10, 12, 9, 6 aromatic), 6.6 (m, C–H11, 20, 22 aromatic), and 3.4 (m, C–H4 aromatic). Furthermore, the singlets for AImP are $\delta(\text{ppm}) = 2.7$ (s, C–H13 aliphatic), 2.9 (m, C–H2 aliphatic), 4.6 (d, C–H4, 8, 9, 12 aromatic), 6.6 (C–H5, 7 aromatic), 7 (d, C–H15 aromatic), and 7.5 (d, C–H17, 16 aromatic). It is evident that molecular conformational differences account for the observed signal disparity. In addition, the ^{13}C NMR (D_2O) of AIP, AMB, and AImP exhibited distinct signals, as depicted in Figure 2 at $\delta(\text{ppm}) = 14$ (C6, C11), 32 (C3), 54 (C2), 114 (C14, C6), 131

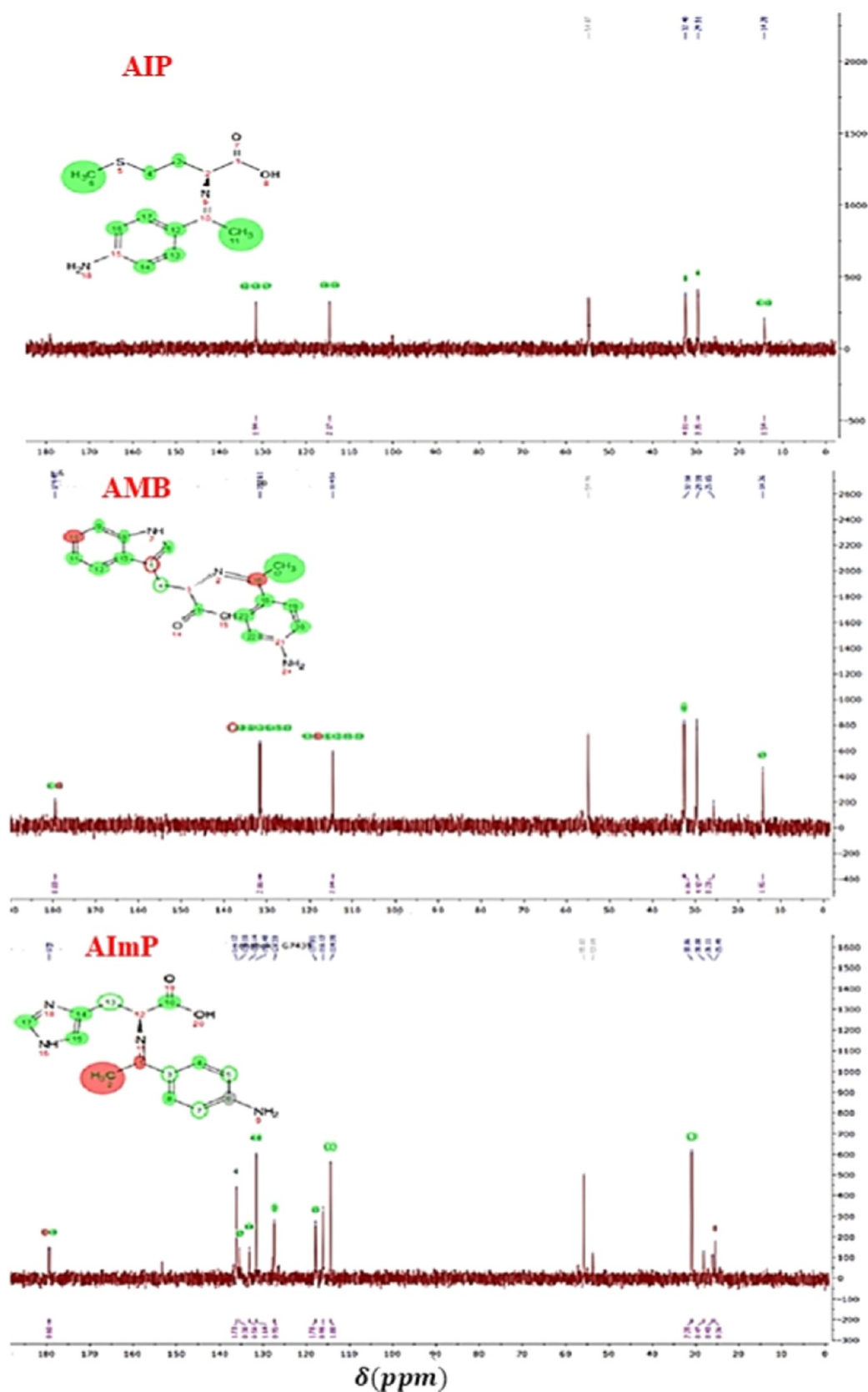


Figure 2. ^{13}C NMR spectra of AIP, AMB, and AImP.

(C12, C13, C17), 29 (C4), and 181 (C1, C13, C17) for AIP and 14 (C17), 32 (C4), 114 (C10, C11, C12, C9, C20, C22), 131 (C8, C6, C5, C13, C23, C19, C18), 117 (C4, C7), and 180 (C101) for the AMB structure. The chemical shift $\delta(\text{ppm}) = 25$

(C2), 30.6 (C13), 113 (C5, C6), 115 (C15), 127 (C4, C8 aromatic), 133 (C14), 135 (C17), and 136 (C6) for the AImP.

3.2. Open Circuit Potential (OCP) Measurements. To investigate the chemical characteristics and corrosion perform-

ance of the Q235 steel alloy, the OCP technique was evaluated as a function of immersion time. The OCP of Q235 steel as a function of the immersion time in 1.0 M HCl solution alone and with the explored inhibitors was measured and referred relative to the SCE electrode within a period of 30 min as presented in Figure 3. In the presence of the explored inhibitors, it is

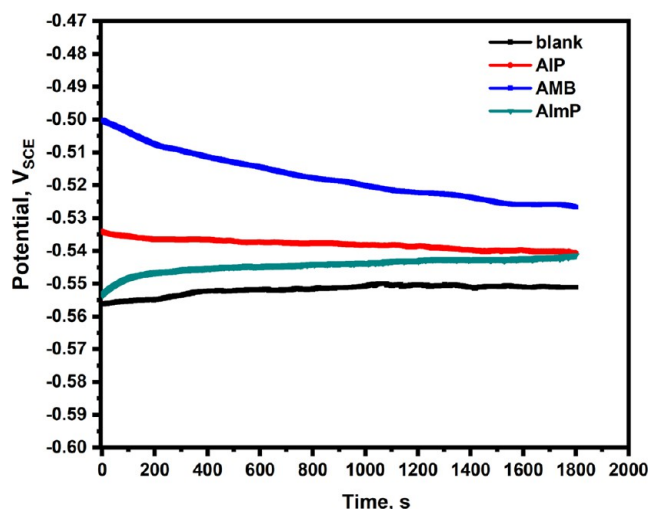


Figure 3. OCP curves measured for Q235 steel in a 1.0 M HCl solution alone and with 10 mM AIP, AMB, and AlmP.

noticeable that the potential sharply shifted toward the more positive side (noble shift), indicating the buildup of a protecting film of the studied compounds on the metallic surface that suppresses anodic corrosion reaction and increases corrosion resistance. The potential values recorded for 1.0 M HCl alone (-0.556) and with 10 mM of AIP, AMB, and AlmP are -0.539 , -0.519 , and -0.544 V_{SCE} , respectively. Accordingly, the effect of the inhibitors on OCP values is noticeable in all explored media, with less negative potentials obtained using the inhibitors compared to their absence, confirming their inhibiting action and the growth of a protective film at the steel/solution interface.²⁸

3.3. Potentiodynamic Polarization. The PDP technique was utilized to investigate the ability of the synthesized inhibitors to hinder the corrosion of Q235 steel in 1.0 M HCl. The PDP curves of the Q235 steel alloy in 1.0 M HCl alone and in the existence of the examined compounds (AIP, AMB, and AlmP) are depicted in Figure 4. The tests were conducted in aerated solutions after 30 min of electrode submerged in the

studied solution to ensure reaching a steady state. The important electrochemical results involving corrosion potential (E_{corr}), and corrosion current density (i_{corr}) were achieved by extrapolation of the cathodic (β_c) and anodic (β_a) Tafel slopes and are summarized in Table 1. The results reveal noticeable changes in the corrosion potential and current values, according to the examined media. The results obviously demonstrate that the addition of the explored compounds resulted in a significant shift in the anodic and cathodic curves toward smaller current densities, implying that the anodic corrosion of Q235 steel and hydrogen ion reduction are retarded or slowed.

The inhibitive effectiveness of the inhibitors to suppress the alloy dissolution was obtained using the polarization curves with the following formula²⁹

$$\eta_{PDP} \% = \frac{i_{corr} - i_{corr(inh)}}{i_{corr}} \times 100 \quad (5)$$

where i_{corr} and $i_{corr(inh)}$ are the corrosion current density in the absence and existence of the examined compounds, respectively.

The existence of the explored compounds increases the protection of steel alloy in HCl media, and as the investigated compound concentration was increased, a marked decrease in corrosion current was observed, with the best inhibition achieved using AMB inhibitor compared to AIP and AlmP owing to the blockage of the active sites on the Q235 steel surface. Moreover, the investigated inhibitors could be categorized as mixed-type inhibitors because their presence causes the corrosion potential values to shift to less negative values with amounts less than 85 mV compared to when they are absent.³⁰

3.4. Electrochemical Impedance Spectroscopy (EIS).

The EIS technique is employed to find clearer insight into the mechanism and kinetics of electrochemical reactions that occur through the corrosion and inhibition processes, as well as to validate the PDP results.³¹ The impedance spectra for bare Q235 steel alone and in the presence of the examined inhibitors (AIP, AMB, and AlmP) in 1.0 M HCl are displayed as Nyquist plots in Figure 5. The dotted lines in this figure characterize the recorded experimental results, and the solid lines correspond to the fitted results. The spectral representation of Nyquist plots shows comparable shapes in the absence and existence of the inhibitors, indicating that these inhibitors do not cause a morphological alteration in the corrosion mechanism. Furthermore, the Nyquist plots in the absence and existence of the inhibitors displayed a single imperfect semicircle, demonstrating

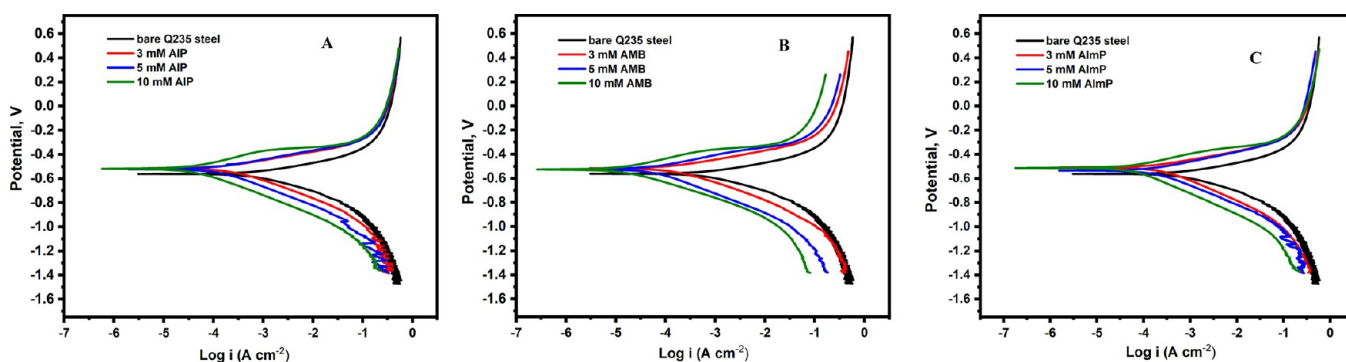


Figure 4. Tafel plots for Q235 steel in 1.0 M HCl in the absence and existence of numerous concentrations of the examined inhibitors AIP (A), AMB (B), and AlmP (C) at 298 K.

Table 1. Electrochemical Parameters for Q235 Steel in 1.0 M HCl in the Existence and Absence of Various Concentrations of AIP, AMB, and AImP Were Achieved by the PDP Technique at 25 °C

inhibitors	conc. (mM)	$i_{\text{corr.}}$ (μA)	$-E_{\text{corr.}}$ (mV)	$\beta_c \times 10^{-3}$ V decade $^{-1}$	$\beta_a \times 10^{-3}$ V decade $^{-1}$	corrosion rate (mpy $^{-1}$)	θ	η_{PDP} (%)
blank		590.0	567.0	116.4	82.50	269.7		
AIP	3	88.90	523.0	130.5	81.90	38.44	0.8493	84.93
	5	65.32	522.0	158.0	83.70	27.07	0.8893	88.93
	10	40.44	519.0	143.3	102.2	18.69	0.9315	93.15
AMB	3	62.91	515.0	165.5	95.60	24.75	0.8934	89.34
	5	45.53	519.0	167.9	86.20	19.97	0.9228	92.28
	10	23.52	518.0	107.6	89.50	10.56	0.9601	96.01
AImP	3	193.2	510.0	144.2	86.10	90.41	0.6725	67.25
	5	162.1	517.0	114.9	74.40	72.12	0.7253	72.53
	10	135.5	530.0	157.1	85.30	61.2	0.7703	77.03

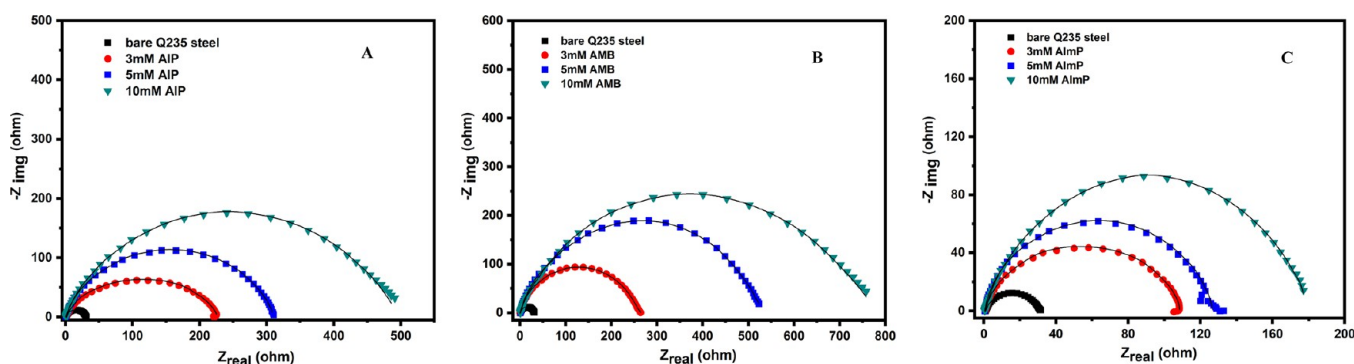


Figure 5. Nyquist plots for bare Q235 steel alone and in the existence of various amounts of the examined compounds AIP (A), AMB (B), and AImP (C) recorded in 1.0 M HCl at 298 K.

that the corrosion process of Q235 steel involves a single charge-transfer operation.

The Nyquist curve of the bare Q235 steel without the examined inhibitors is characterized by a depressing shape of semicircles in the high-frequency range, which signifies the roughness of steel alloy.³² When the investigated inhibitors were added, the semicircle shape of Nyquist spectra increased in comparison to the inhibitor's free media, revealing their adsorption on the steel surface producing a compact protective film with higher impedance for the charge-transfer process, leading to a reduction in the corrosion process. Impedance curves grew in diameter when inhibitors were added and increased more with increasing their concentration; the AMB impedance curve exhibited the largest increase in diameter, followed by AIP and then AImP.

Figure 6 depicts a schematic representation of the equivalent circuit employed to fit the EIS results. The circuit consists of solution resistance (R_s), charge-transfer resistance (R_{ct}), and double-layer capacitance (C_{dl}). To accomplish a precise fit for the results, R_{ct} was changed with a constant phase element (CPE).

The impedance of CPE (Z_{CPE}) is illustrated in the following equation³³

$$Z^{\text{CPE}} = \frac{1}{[Y^0(j\omega)^n]} \quad (6)$$

where Y^0 is the CPE constant, j is the imaginary number, ω is the angular frequency (measured in rad s $^{-1}$), and n is the shift in phase.

The resulting values could be used to clarify the morphological characteristics of metal surfaces deteriorated in corrosive solution. A larger value typically denotes significant

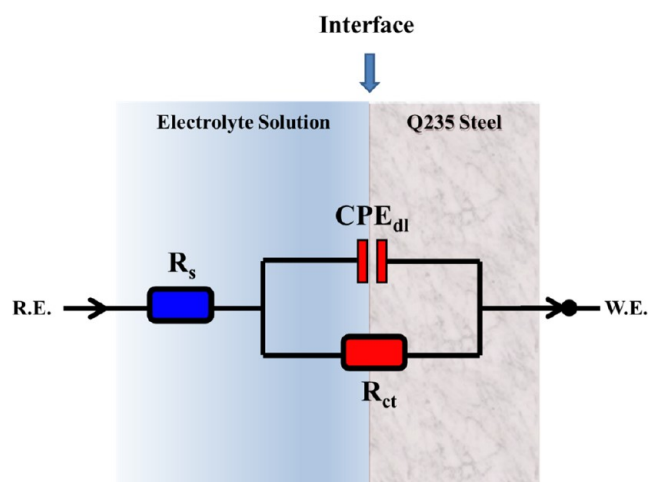


Figure 6. Equivalent circuit was utilized to fit the impedance results of the bare steel alloy.

smoothness of the surface. Additionally, when $n = 0$ and $Y^0 = R$, the CPE denotes a resistive behavior. However, if $n = 1$ and $Y^0 = C$, the CPE indicates capacitance. Meanwhile, if $n = 0$ and $Y^0 = 1/L$, the CPE will denote an inductive behavior. Finally, when $n = 1/2$ and $Y^0 = W$, the CPE describes a Warburg impedance.

The protection efficiency (η_{EIS} %) for Q235 steel corrosion was calculated using the R_{ct} values as shown below³⁴

$$\eta_{\text{EIS}} \% = \frac{R_{ct(\text{inh})} - R_{ct}}{R_{ct(\text{inh})}} \times 100 \quad (7)$$

Table 2. Electrochemical Data Accomplished by the EIS Method for the Corrosion of Bare Q235 Steel Alloy alone and Inhibited with Numerous Concentrations of AIP, AMB, and AImP in 1.0 M HCl^a

inhibitor	conc. (mM)	R_s (Ω cm ²)	R_{ct} (Ω cm ²)	n	C_{dl} (μ F cm ⁻²)	θ	η_{PDF} (%)	φ^2
blank		1.83	33	0.79	119.3			
AIP	3	1.98	227	0.85	53.4	0.8546	85.46	0.00074
	5	2.12	281	0.88	44.3	0.8862	88.62	0.00065
	10	2.35	453	0.90	35.2	0.9271	92.71	0.00096
AMB	3	2.41	261	0.96	41.3	0.8736	87.36	0.00078
	5	1.80	525	0.92	32.1	0.9371	93.71	0.00054
	10	1.94	775	0.91	28.6	0.9574	95.74	0.00051
AImP	3	2.13	108	0.81	73.6	0.6944	69.44	0.00056
	5	2.45	124	0.80	69.4	0.7339	73.39	0.00078
	10	2.22	171	0.83	58.2	0.8070	80.70	0.00089

^a φ^2 is the goodness of the fit.

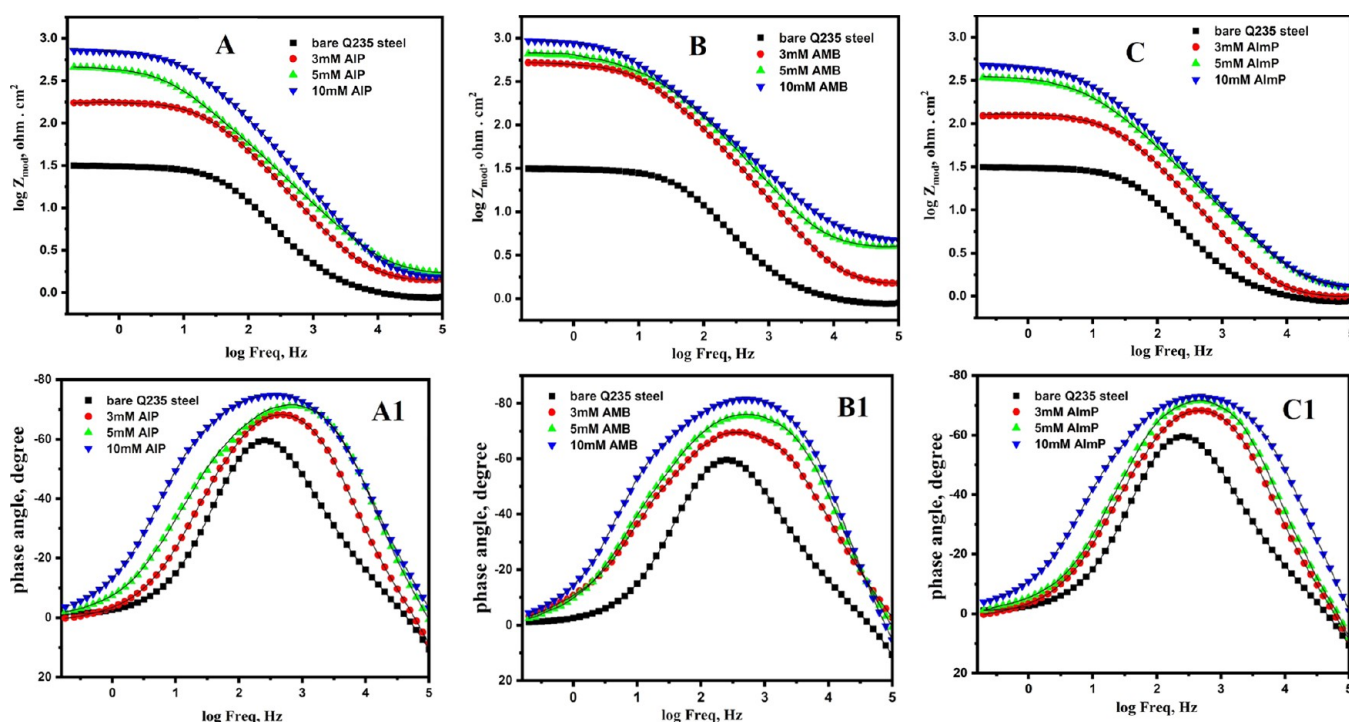


Figure 7. Bode (A–C) and bode phase (A1–C1) plots for bare Q235 steel alone and in the existence of numerous amounts of AIP, AMB, and AImP, respectively, recorded in a 1.0 M HCl solution at 298 K.

where R_{ct} and $R_{ct(inh)}$ are the charge-transfer resistances estimated in the absence and existence of the explored inhibitors, respectively.

The R_{ct} values recorded in Table 2 were determined from Nyquist plots by subtracting the impedance at the smaller and greater frequencies. A significant increase in the R_{ct} value was monitored in the presence of the investigated inhibitors in comparison with the uninhibited steel alloy. From Table 2 and Figure 5, it is apparent that with the increase of the investigated compound concentration, the R_{ct} values were increased, while the Y^0 values corresponding to CPE_{dl} declined. This suggests that the adsorbed molecules of the investigated compounds on the metallic surface gradually increased and thus diminished the active sites that initiate the dissolution reaction. Furthermore, increasing R_{ct} demonstrated a significant inhibition of charge transfer in the protecting film caused by the adsorbed inhibitor on the steel surface, demonstrating excellent resistance to acidic attack and, as a result, controlling the extent of dissolution. Additionally, the values of C_{dl} have decreased as a result of the

dielectric constant decline and/or the increase in the electric double-layer thickness caused by the adsorption of the examined compounds at the steel/electrolyte interface.^{35,36}

The Bode plots (impedance and phase angle vs frequency) for Q235 steel in 1.0 M HCl in the absence and existence of numerous amounts of AIP, AMB, and AImP are presented in Figure 7. The diagrams were used to understand the behavior of the adsorbed inhibiting film at the Q235 steel surface. The addition of the explored inhibitors showed a higher impedance value because of the difficulties of reacting at the interface. Moreover, a decrease in the phase angle value is less than 90°, demonstrating the roughness of the steel surface and its porous state because of the efficient adsorption of the explored inhibitors on the steel surface. The maximum impedance was recorded in the existence of the AMP inhibitor at the low-frequency region and increased with increasing its concentration, which granted the greatest corrosion inhibition to the steel alloy.

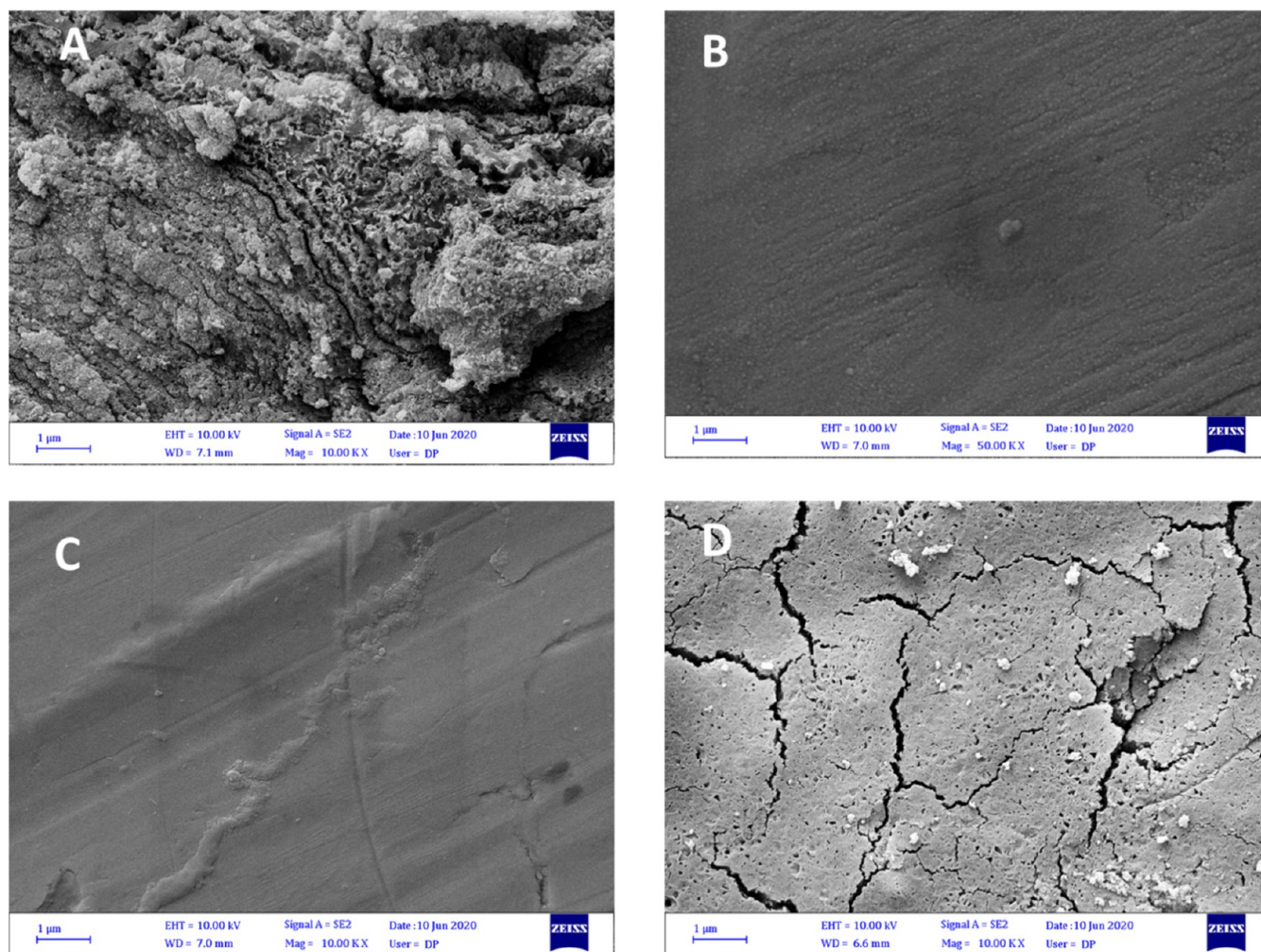


Figure 8. SEM images for the Q235 steel surface after dipping for 48 h in a 1.0 M HCl solution alone (A) and with 10 mM AIP (B), 10 mM AMB (C), and 10 mM AImP (D).

In conclusion, the EIS and PDP results are in harmony, proving the pronounced effect of the explored inhibitors that can greatly enhance the anticorrosion performance of the Q235 steel alloy in acidic media.

3.5. SEM and EDS Analyses. The surface morphologies of Q235 steel samples were evaluated via SEM measurements after dipping in the corrosive medium (1.0 M HCl) alone and containing the investigated inhibitors (AIP, AMB, and AImP), and the SEM micrographs of the surfaces are presented in Figure 8. The metallic surface of steel after dipping in the aggressive media in the absence of a corrosion inhibitor is shown in Figure 8A in which a highly corroded surface was observed because of the destructive attack of the acidic solution on the steel specimen. Moreover, the surface was severely damaged and appeared to have apparent imperfections due to the corrosion process. In the case of steel samples submerged in HCl with 10 mM of the explored inhibitors, the surface morphology is obviously different, as depicted in Figure 8B–D. In the existence of AIP and AMB, the surfaces became smoother as well as less damaged compared with the surface immersed in HCl alone. This is caused by the formation of an inhibiting layer adsorbed on the steel surface, which maintains the original surface state and thus inhibits corrosion. In the presence of AImP (Figure 8D), the cracks observed in the formed layer are probably caused by internal stresses that manifest as the thickness increases.

Generally, it is evident according to the aforementioned images that their order of inhibition ability is $AMB > AIP > AImP$, which is compatible with the electrochemical findings.

Figure 9 shows EDS spectra for Q235 steel after 48 h of immersion in 1.0 M HCl containing the optimum concentration (10 mM) of the investigated inhibitors (AIP, AMB, and AImP) at room temperature. The spectrum after immersion in 1.0 M HCl alone (Figure 9A) shows signals for Fe, C, and O related to the elements of the oxide film formed owing to the corrosion product buildup on the metallic surface. In the existence of the examined inhibitors (Figure 9B–D), it was obvious that the signals in the EDS spectrum associated with the corrosion products approximately diminished, and the appearance of peaks related to the inhibitors confirmed their effective adsorption on the metallic surface and suppression of steel corrosion in the corrosive solution. The intensity of the signal height of elements related to the inhibitors is higher in the presence of AMB than in the case of AIP and finally AImP, demonstrating the formation of a more intense film in the existence of AMB, which agrees with the SEM observations.

In addition, EDS mapping analyses of the steel surface after 48 h of immersion in 1.0 M HCl in the absence and existence of the explored compounds are displayed in Figure 10. The figure depicts a uniform distribution of inhibitor elements on the alloy surface in the existence of the inhibitors. In general, the EDS

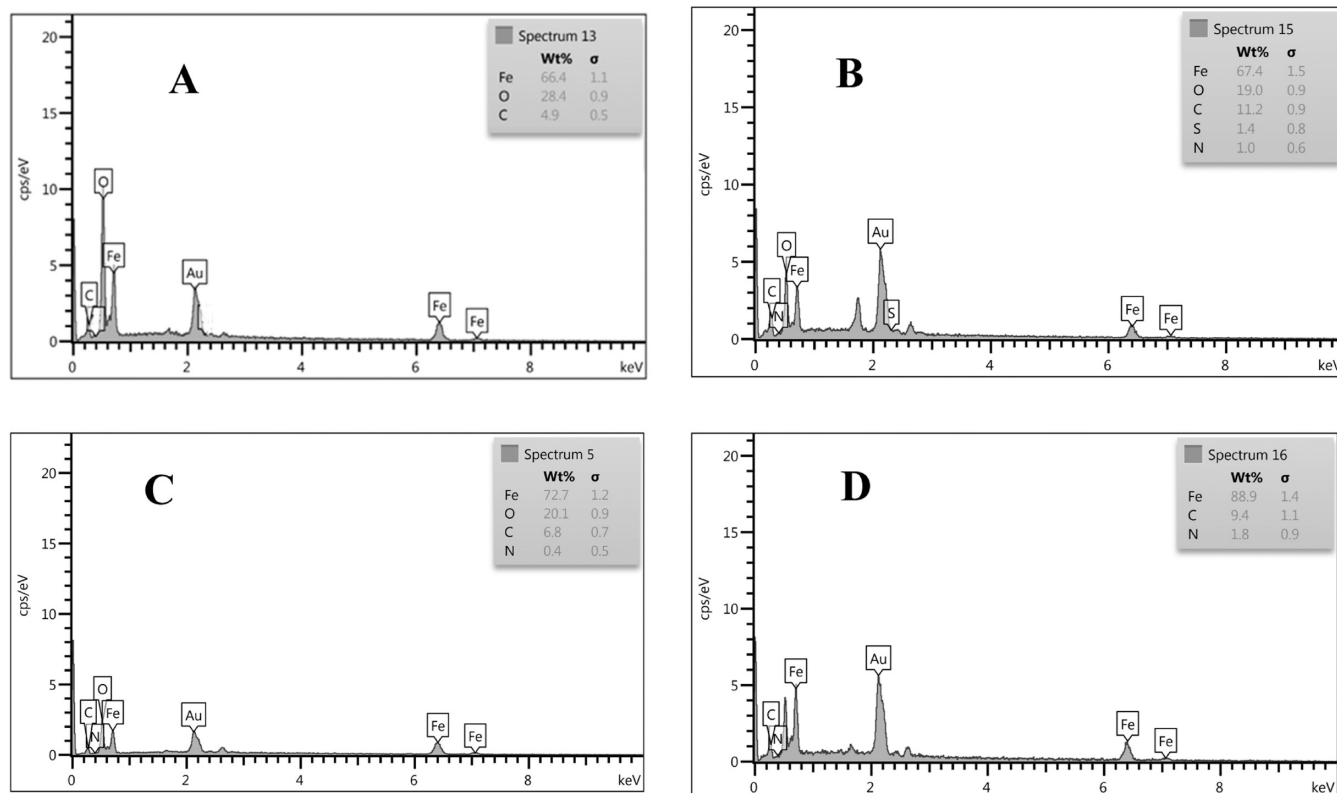


Figure 9. EDS spectra for the Q235 steel surface after dipping for 48 h in a 1.0 M HCl solution alone (A) and with 10 mM AIP (B), 10 mM AMB (C), and 10 mM AImP (D).

spectrum and mapping display clear evidence of decreased corrosion products and the development of the inhibited film on the steel surface in the presence of the explored inhibitors.

3.6. Fourier-Infrared Spectroscopic Studies. To illustrate the adsorption process of the investigated compounds on the Q235 steel surface, the FTIR technique was used to examine the inhibitors and the film growth on the steel surface after dipping in 1.0 M HCl containing the inhibitors as depicted in Figure 11. The FTIR spectra of pure AIP shown in Figure 11A showed an absorption band at 3402 cm^{-1} owing to the N–H and a wide band at 3224 cm^{-1} related to the CO–OH bond of the carboxylic acid. Also, an absorption band at 1690 cm^{-1} refers to the stretching of the imine group (C=N), and the band at 1843 cm^{-1} refers to the stretching of the C=O bond of the carboxylic acid. Also, for the bending band at 1650 cm^{-1} , absorption bands at 1404 and 1449 cm^{-1} have been allocated to the N–H, O–H, and C–S, respectively. In the case of the film grown on the alloy surface immersed in AIP, the spectrum showed the most important band at 3419 cm^{-1} that was allocated to the N–H amino bond, the band at 1633 cm^{-1} related to the bending N–H amino bond, and the band at 1449 cm^{-1} refers to the bending of the O–H of the carboxylic acid, and at 1383 cm^{-1} due to the stretching of the C–N amino bond, and at 670 cm^{-1} matches to the bending of the C–H of the 1,4-disubstituted aromatic ring.

The FTIR spectrum for ABM (Figure 11B) displays characteristic peaks to the N–H stretching of the amino group at (3402 cm^{-1}), the aromatic N–H stretching at (3670 cm^{-1}), the CO–OH stretching at (3224 cm^{-1}), the stretching of the imine group C=N at (1635 cm^{-1}), the C=O stretching for the carboxylic acid at (1875 cm^{-1}), the aromatic C–H bending at (2052 and 840 cm^{-1}), the N–H bending at (1650 cm^{-1}), and the O–H bending of the carboxylic acid at (1437 cm^{-1}). For the

film that developed at the alloy surface immersed in ABM, the spectrum shows a broad band due to O–H stretching at (3421 cm^{-1}), C=N stretching at (1732 cm^{-1}), and aromatic C–N stretching at (1332 cm^{-1}).

The FTIR spectrum shown in Figure 11C for AImP presented absorption bands representative of the aromatic N–H at (3749 cm^{-1}), N–H stretching of the amino group at (3394 cm^{-1}), CO–OH bond stretch of the carboxylic acid at (3232 cm^{-1}), stretching the imine group C=N at (1635 cm^{-1}), stretching C=O of carboxylic acid at (1870 cm^{-1}), bending N–H at (1650 cm^{-1}), and O–H bending at (1434 cm^{-1}). Moreover, the FTIR spectrum for the film of AImP shows a broad band for the O–H stretching of the H atom at (3393), the C=N stretching at (1731), and the bending of the N–H bond at (1635).

Comparing the FTIR spectra in Figure 11 proves the adsorption of the explored compounds on the alloy surface, and the shift in some peaks demonstrates that the functional groups in the investigated inhibitors are responsible for this adsorption.

3.7. UV–Visible Spectroscopy. UV–visible spectroscopy was used to get a better understanding of the interactions among the steel alloy and the AIP, AMB, and AImP molecules. The absorption spectra of the steel surface prior to and after 48 h of steel immersion in 1.0 M HCl in the absence and existence of 10 mM of the examined compounds are displayed in Figure 12. As shown in Figure 12A, the UV spectrum for AIP before immersion had the highest absorbance band at 229 nm and another band at 268 nm owing to the electronic transitions $n-\pi^*$ and $\pi-\pi^*$ of the imine group (C=N) and the aromatic ring, respectively. After the immersion stage, the highest value of the absorbance was at 228 nm, and the other peak was at 282 nm. The increase in the intensity of the absorbance resulted from the

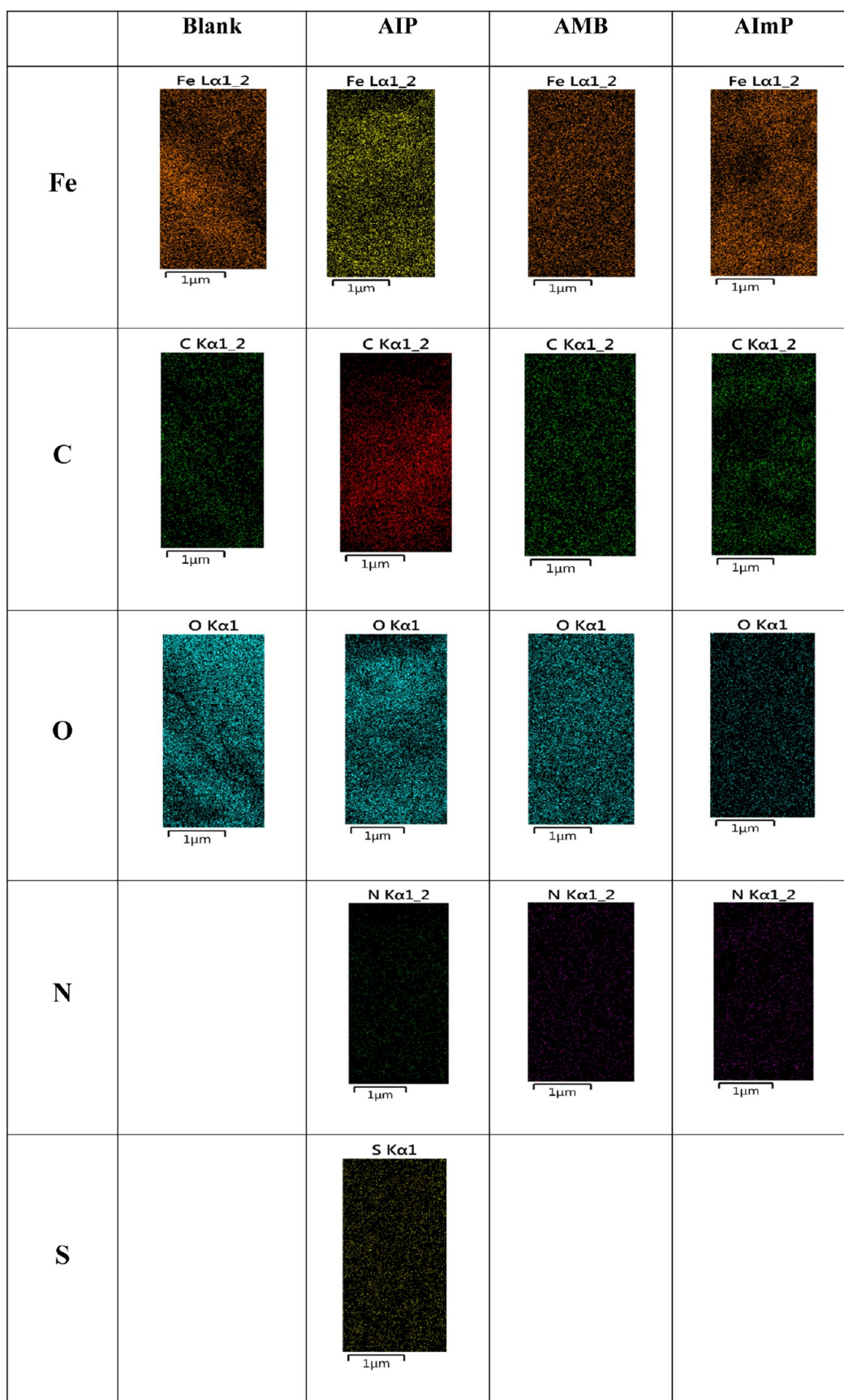


Figure 10. EDS mapping of the Q235 steel surface after dipping for 48 h in 1.0 M HCl alone (blank) and with 10 mM AIP, 10 mM AMB, and 10 mM AlmP.

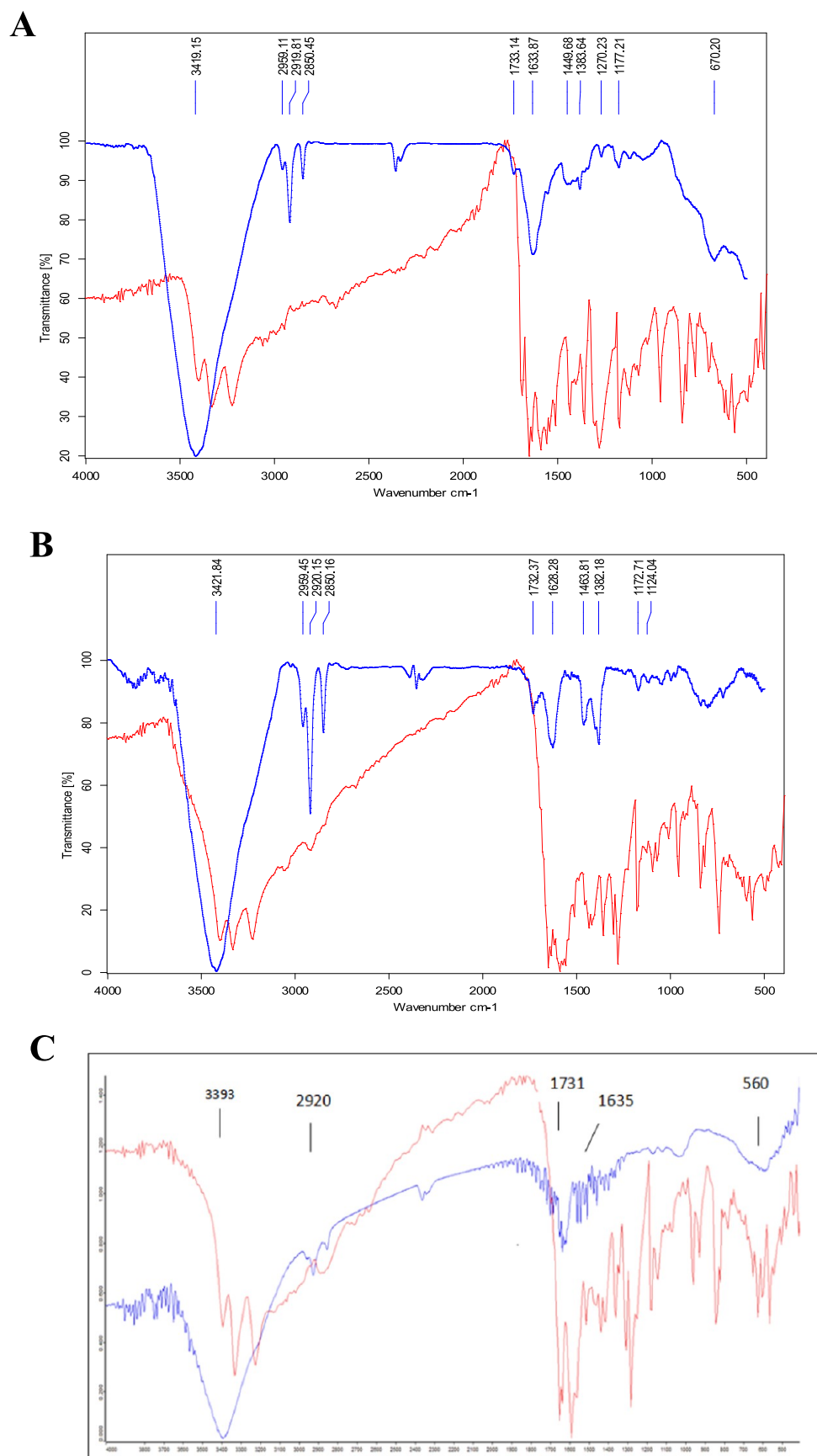


Figure 11. FTIR spectra of the pure inhibitors (red) and the film formed on the Q235 steel surface (blue) after dipping for 48 h in 1.0 M HCl containing AIP (A), AMB (B), and AlmP (C) at 298 K.

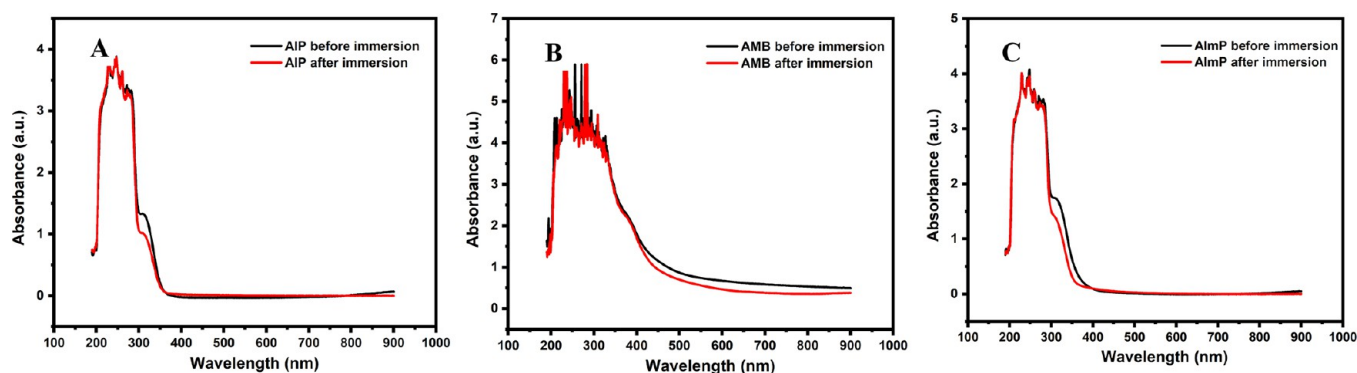


Figure 12. Results of UV–visible tests of the examined inhibitors **AIP** (A), **AMB** (B), and **AImP** (C) before and after immersion in HCl solution.

hyperchromic effect. **Figure 12B** shows the absorption spectra of the **AMB** inhibitor before the steel immersion in which the highest absorbance peak is at 232 nm and other peaks are at 256 and 271 nm owing to the electronic transitions $n-\pi^*$ and $\pi-\pi^*$ of the imine group (C=N) and the transitions of the aromatic rings. After the immersion, the highest value of the absorbance was at 232 nm, while the other peaks were at 279 and 236 nm, with the absorption shift toward a higher wavelength (red shift), which was assigned to the $\pi-\pi^*$ transition of the C=C bonds existing in the examined inhibitor. In the case of **AImP** (**Figure 12C**), the UV spectrum before immersion showed the highest absorbance at 229 nm and another band at 252 nm because of the electronic transitions $n-\pi^*$ and $\pi-\pi^*$ of the imine group (C=N) and the aromatic ring, respectively. After immersion, the highest absorbance was recorded at 248 nm and the other one at 281 nm. The increase in the intensity of the absorbance resulted due to the hyperchromic effect, with a red shift in the absorption because of the $\pi-\pi^*$ transition resulting from the double bonds in the aromatic rings of **AImP**. According to the results recorded for the three inhibitors, the displacement (red shift) in the spectra with the decrease in the absorbance values suggests complex formation among the explored inhibitors and the steel surface, which is the indication of the sorption mechanism of inhibitors on the steel resulting in the corrosion mitigation.^{37,38}

3.8. XPS Analysis. The XPS technique was utilized to distinguish the chemical composition and declare the bonding state of the studied inhibitor **AMB**. The XPS survey spectra of Q235 steel were recorded after immersion in a 1.0 M HCl solution containing 10 mM of **AMB** for 24 h as depicted in **Figure 13**. The presence of C, N, O, Cl, and Fe elements in XPS results with using the inhibitor provided evidence for the adsorption of **AMB** on the steel surface and the formation of a protective film. To get a more in-depth understanding of the interaction among **AMB** and steel surface and to explore the existence form of these elements, the XPS spectra of the recorded elements and their fitting results are presented in **Figure 13**.

Figure 13 shows the deconvoluted C 1s spectrum, which revealed three distinct peaks at 284.5 eV (C–C, C–H, and C=C) and 286.2 eV (C–N and C=N), and the third peak at 288.4 eV is attributed to the formation of a C–N⁺ species, which probably resulted from the N atom protonation and/or the N coordination with iron (N–Fe).³⁹ The O 1s spectrum is deconvoluted into two peaks at 530.07 and 531.5 eV, corresponding to FeO/Fe₂O₃ (at 530.07) and FeOOH (at 531.5 eV) as shown in **Figure 13**. The Fe 2p_{3/2} spectrum (**Figure 13**) shows six peaks at 711.06 eV (Fe 2p_{3/2} of Fe²⁺), 714.54 eV

(Fe 2p_{3/2} of Fe³⁺), 719.05 eV (Fe 2p_{3/2} satellites of Fe²⁺), 724.04 eV (Fe 2p_{1/2} of Fe²⁺), 727.9 eV (Fe 2p_{1/2} level of Fe³⁺), and 732.4 eV (Fe 2p_{3/2} satellites of Fe³⁺). The deconvolution of the Cl 2p spectrum reveals two peaks at 198.6 eV (NaCl) and 200.2 eV (FeCl₂, FeCl₃), which have been assigned to Cl 2p_{3/2} and Cl 2p_{1/2}, respectively (**Figure 13**). The peak observed at 200.2 eV is attributed to the existence of ferrous/ferric chlorides, which suggest the chemisorption of chloride on the steel surface.⁴⁰ Moreover, the N 1s spectrum deconvoluted into three peaks at 399.7, 400.1, and 401.2 eV belonging to both neutral and protonated N components in the adsorbed film (**Figure 13**). The peak at 399.7 eV corresponds to a C–N bond, while the peak at 400.1 eV is related to N–Fe. The presence of the N–Fe bond suggests the chemical adsorption of **AMB** on the Q235 steel surface. The third peak identified at 401.2 eV is attributed to the existence of the positively charged N in the form of (=N⁺ + H[−]), which indicate the physical adsorption of **AMB** on the surface of Q235 steel.⁴¹ Finally, the results suggest that the investigated inhibitor **AMB** is able to form a protective layer on the steel surface via both chemical and physical adsorption mechanisms, which can efficiently control steel corrosion.

3.9. DFT Calculations. Molecular structures, lowest unoccupied molecular orbital (LUMO), and highest occupied molecular orbital (HOMO) distributions, and the theoretical parameters for **AIP**, **AMB**, and **AImP** are exhibited in **Figure 14** and **Table 3**, respectively. According to the Frontier molecular orbital (FMO) theory, the ability of donor or acceptor interactions occurring on the surface of an additive/metal is illustrated by its LUMO and HOMO energy levels.^{26,42,43} Hence, an inhibitor molecule with high E_{HOMO} and small E_{LUMO} values is superior to inhibiting corrosion. From **Table 3**, the **AMB** molecule has the greatest E_{HOMO} value of −4.69 eV compared to those of **AIP** and **AImP** molecules (−4.76, −4.88 eV). **Figure 14** reveals that the HOMO level for the inhibitor molecules is located on the amino, imine groups, indole, imidazole moieties, and phenyl rings, revealing that these locations are more susceptible to electrophilic attacks on the Q235 steel surface. These explanations corroborate the experimental findings that the molecules of the explored compounds are capable of being adsorbed on the surface of Q235 steel, hence increasing the protection efficiency. Nevertheless, **Table 3** shows that the **AMP** molecule has a lower E_{LUMO} value (−1.98 eV) than the **AIP** and **AImP** molecules (−1.85, −1.79 eV). The low E_{LUMO} value for the **AMB** molecule confirms previous findings, suggesting that it has excellent protective properties.

Also, lowering the energy gap (ΔE) is important since it increases the inhibitor additive's corrosion–prevention proper-

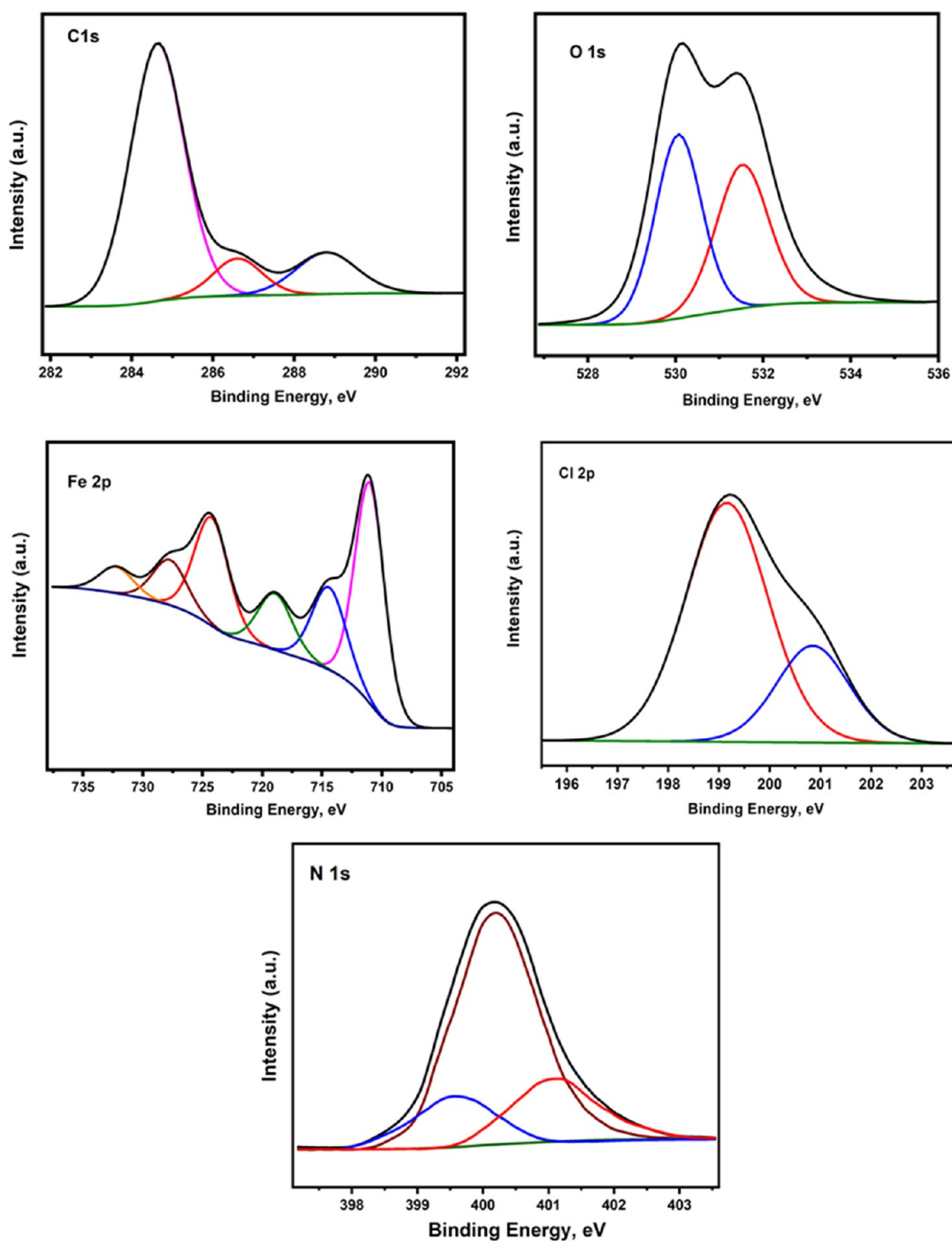


Figure 13. XPS spectra of Q235 steel in a 1.0 M HCl solution containing 10 mM of AMB: C 1s, O 1s, Fe 2p, Cl 2p, and N 1s.

ties.²⁷ According to Table 3, the ΔE value for the AMB molecule (2.71 eV) is lesser than that of the AIP and AIMP molecules (2.91 and 3.09 eV), making it more probable that the AMB molecule will be adsorbed on the Q235 steel interface.

Commonly, the inhibitors' capability to deliver electrons to the Q235 steel surface is often shown by relatively low electronegativity (χ) values.⁴⁴ In contrast, inhibitor molecules with large electronegativity have a better chance of receiving an electron from the Q235 steel interface (this process is known as "back-donation") and forming a stronger connection with the Q235 steel surface.⁴⁵ Table 3 demonstrates that AIP, AMB, and

AIMP molecules have somewhat high electronegativity, suggesting that they have the back-donation possibility to form a more robust bond with Q235 steel's interface.

Furthermore, softness (σ) and hardness (η) are measures of the stability and reactivity of inhibitor molecules. The soft molecules exhibit a stronger protective capability compared to those of hard molecules because of the smooth transport of electrons to the Q235 steel contacted through the adsorption, making them powerful corrosion inhibitors.⁴⁶ As represented in Table 3, the AMB molecule exhibits superior inhibitory

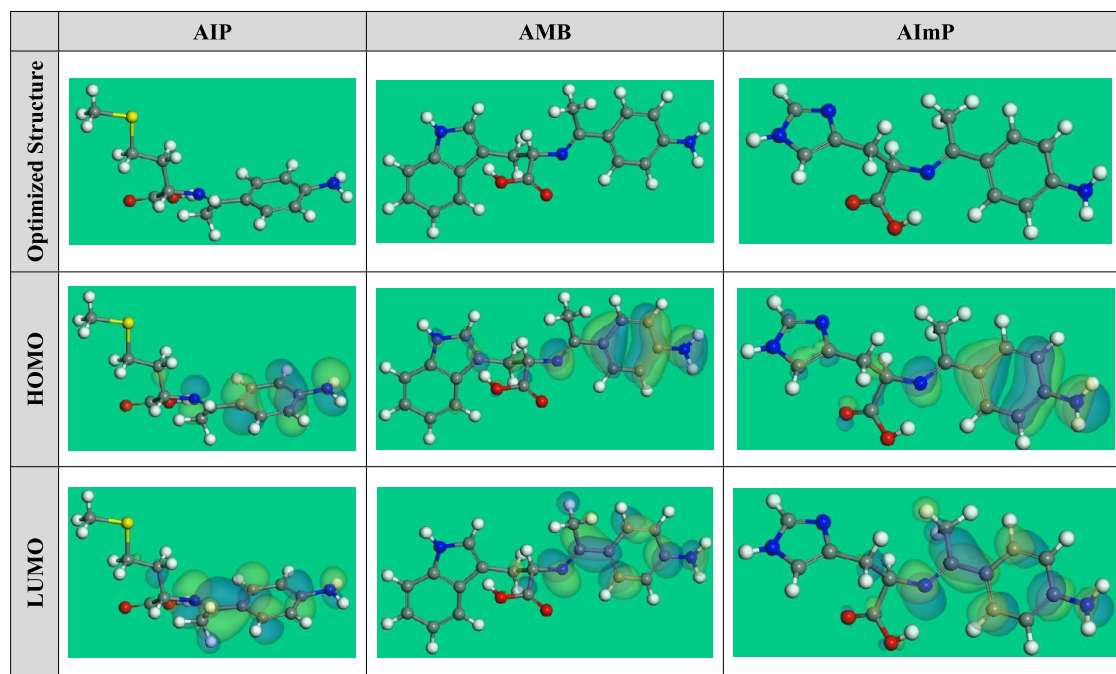


Figure 14. Optimized structure and HOMO and LUMO orbital occupation for the explored **AIP**, **AMB**, and **AImP** compounds utilized by the DFT approach.

Table 3. DFT Parameters of the Investigated **AIP**, **AMB**, and **AImP** Molecules

parameters	AIP	AMB	AImP
E_{HOMO} (eV)	-4.76	-4.69	-4.88
E_{LUMO} (eV)	-1.85	-1.98	-1.79
$\Delta E = E_{\text{LUMO}} - E_{\text{HOMO}}$ (eV)	2.91	2.71	3.09
electronegativity (χ)	3.31	3.34	3.34
global hardness (η)	1.45	1.36	1.55
global softness (σ)	0.69	0.74	0.65
the number of electrons transferred (ΔN)	1.27	1.35	1.18
$\Delta E_{\text{back-donation}}$	-0.36	-0.34	-0.39
dipole moments (μ) (debye)	8.72	9.74	7.88
molecular surface area (\AA^2)	301.43	348.91	297.18

characteristics due to its higher σ value and lower η value when compared to those of the **AIP** and **AImP** molecules.

Moreover, the inhibitor's capacity for electron donation or acceptance is assessed by the fraction of electron transfer (ΔN) and $\Delta E_{\text{back-donation}}$. This means that if the values of ΔN are more than zero, it is likely that electrons will transfer from the inhibitor molecule to the Q235 steel interface atoms and vice versa if the values of ΔN are lower than zero (i.e., back-donation).⁴⁷ Table 3 displays that the ΔN values for the investigated molecules are all higher than zero, indicating that **AIP**, **AMB**, and **AImP** molecules are proficient for providing electrons to the Q235 steel surface, besides the **AMB** molecule having a better donation ability than either **AIP** or **AImP**. Furthermore, when $\Delta E_{\text{back-donation}}$ is less than zero, the withdrawn electron from the Q235 steel surface atoms will be pursued by a back-donation from the molecule to the Q235 steel interface atoms, and this is the dynamically favored state.⁴⁸ Table 3 exhibits that the $E_{\text{back-donation}}$ values for **AIP**, **AMB**, and **AImP** molecules are all negative, indicating that back-donation is desirable for these molecules in order to build a strong connection with the Q235 steel interface.⁴⁹

The dipole moment is also a crucial parameter that is used in the corrosion protection prognosis approach.⁵⁰ The molecule's adsorption on the metallic surface is enhanced, and the distortion energy is augmented by the increase in dipole moment. Hence, an enhancement in dipole moment results in better corrosion inhibition.⁵¹ Table 3 displays that the high dipole moment value of the **AMB** molecule (9.74 debye) is compared to that of the **AIP** and **AImP** molecules (8.72 and 7.88 debye values), which gives the **AMB** molecule a greater tendency to be adsorbed on the Q235 steel surface and increases the corrosion protection.

In addition, the propensity of **AIP**, **AMB**, and **AImP** molecules to protect Q235 steel in corrosive media is directly correlated to their molecular surface area. The increase in the contact area among the inhibitor molecules and the metal surface led to greater efficacy in inhibition. As shown in Table 3, the molecular surface area of the **AMB** molecule (348.91 \AA^2) is significantly higher than that of the **AIP** and **AImP** molecules, making it a more effective inhibitor.

Additionally, the Dmol³ module assesses molecular electrostatic potential (MEP) mapping, which might discover the active sides of inhibitor species. The MEP mapping is a 3D visual indicator applied to recognize the total charge distribution's influence totally on a molecule.⁵² The high electron density region, where the MEP is extremely negative (nucleophilic reaction), is described by the red color in the MEP maps displayed in Figure 15. On the other hand, the region with the most positivity is represented by the blue colors (electrophilic interaction).⁵³ The optical analysis of Figure 15 confirms that the nitrogen atoms in the amino and imine groups have a higher electron density than the oxygen atoms in the carboxylic groups. The areas with higher electron densities in inhibitor species (i.e., the red area) might be the most appropriate for attracting steel interfaces and producing robust adsorbed protective layers.

3.10. MC Simulations. A clear idea of the adsorption mechanism was also suggested by MC simulations, which were

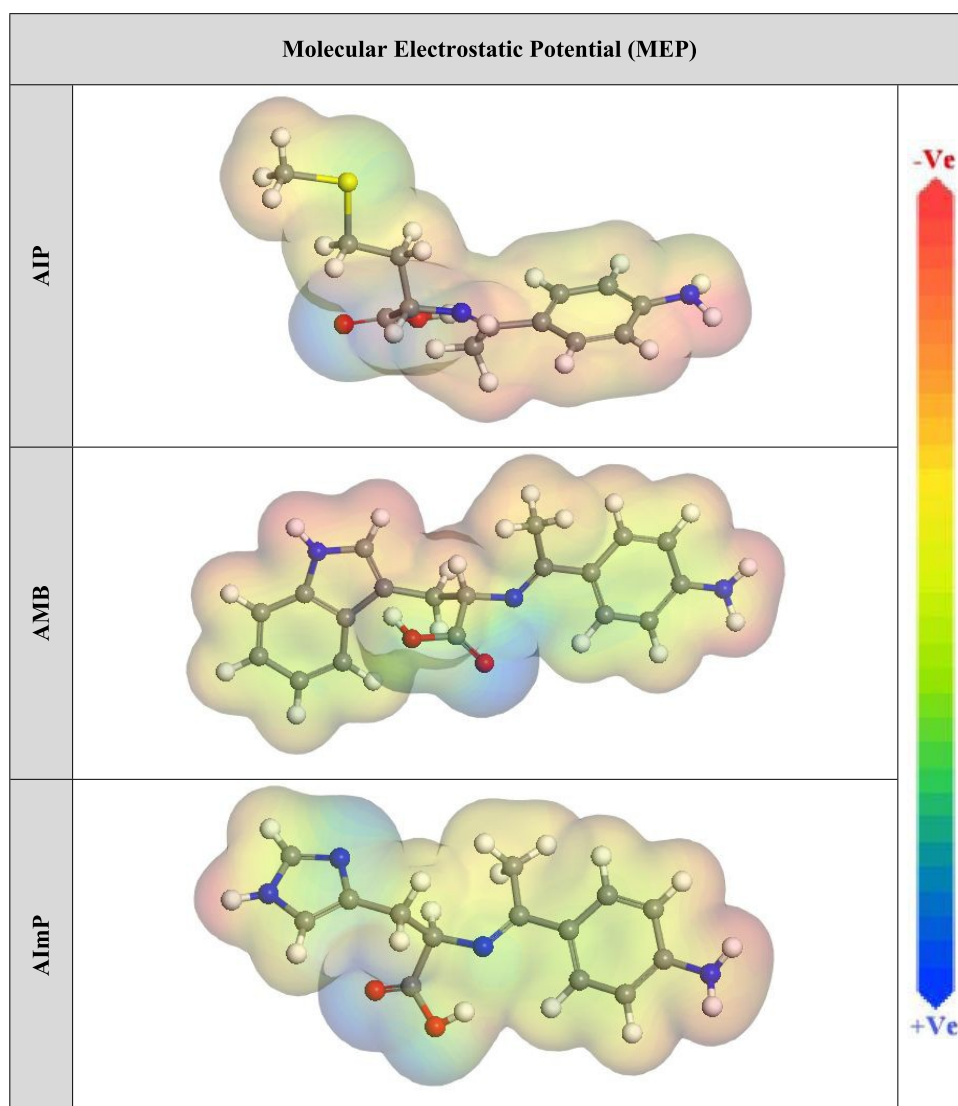


Figure 15. Graphical presentation of the MEP of the investigated **AIP**, **AMB**, and **AImP** compounds utilized by the DFT approach.

devoted to identifying the affinities of the inhibitor species with the steel surface. Therefore, the adsorption locator module accomplishes the greatest appropriate adsorption configurations for the **AIP**, **AMB**, and **AImP** molecules on the Q235 steel interface in HCl media (Figure 16), that is, appearing in a roughly flat disposition, designating an enhancement in the adsorption and greatest surface coverage.⁵⁴ Furthermore, Table 4 displays the adsorption energies determined using the MC simulations. From the table, it was observed that the **AMB** molecule ($-3286.05 \text{ kcal mol}^{-1}$) has greater negative adsorption energy in comparison with the **AIP** and **AImP** molecules (-3212.23 , $-3174.46 \text{ kcal mol}^{-1}$). These results are in accord with the experimental results and presume that the energetic adsorption of the **AMB** on the Q235 steel interface gives rise to the construction of a stable adsorbed film that inhibits the Q235 steel from corrosion.⁵⁵ Moreover, the adsorption energy values for the **AMB** molecule in both the unrelaxed ($-3100.53 \text{ kcal mol}^{-1}$) and relaxed ($-185.52 \text{ kcal mol}^{-1}$) states are more negative compared to the **AIP** and **AImP** molecules as shown in Table 4, corroborating that the **AMB** molecule has a larger protective performance than the **AIP** and **AImP** molecules.

The dE_{ads}/dN_i values assist in clarifying the metal/adsorbate arrangement energy if the adsorbed inhibitor molecule or the molecules of other adsorbates were eliminated.⁵⁶ Table 4 reveals that the dE_{ads}/dN_i values of **AMB** molecules ($-306.61 \text{ kcal mol}^{-1}$) are greater than those of **AIP** and **AImP** molecules (-284.47 , $-261.27 \text{ kcal mol}^{-1}$), indicating that **AMB** molecules exhibit superior adsorption. In addition, the dE_{ads}/dN_i values are around -15.42 for water molecules, -64.37 for hydronium ions, and -105.53 for chloride ions. These values are much smaller compared to those of **AIP**, **AMB**, and **AImP** molecules, implying that inhibitor molecules are strongly adsorbed and easily outcompete H_2O molecules, hydronium ions, and chloride ions. Thus, both experimental and theoretical research agree that the molecules of **AIP**, **AMB**, and **AImP** are effectively adsorbed on the surface of the Q235 steel, creating a potent adsorbed layer that shields the alloy from corrosion in a corrosive medium.

3.11. Mechanism of Corrosion Inhibition. It is critical to understand the mechanism of corrosion protection provided by the explored organic inhibitors on the Q235 steel surface under the corrosive acidic conditions studied. The corrosion process of steel in the acidic solution involves an anodic process (metallic

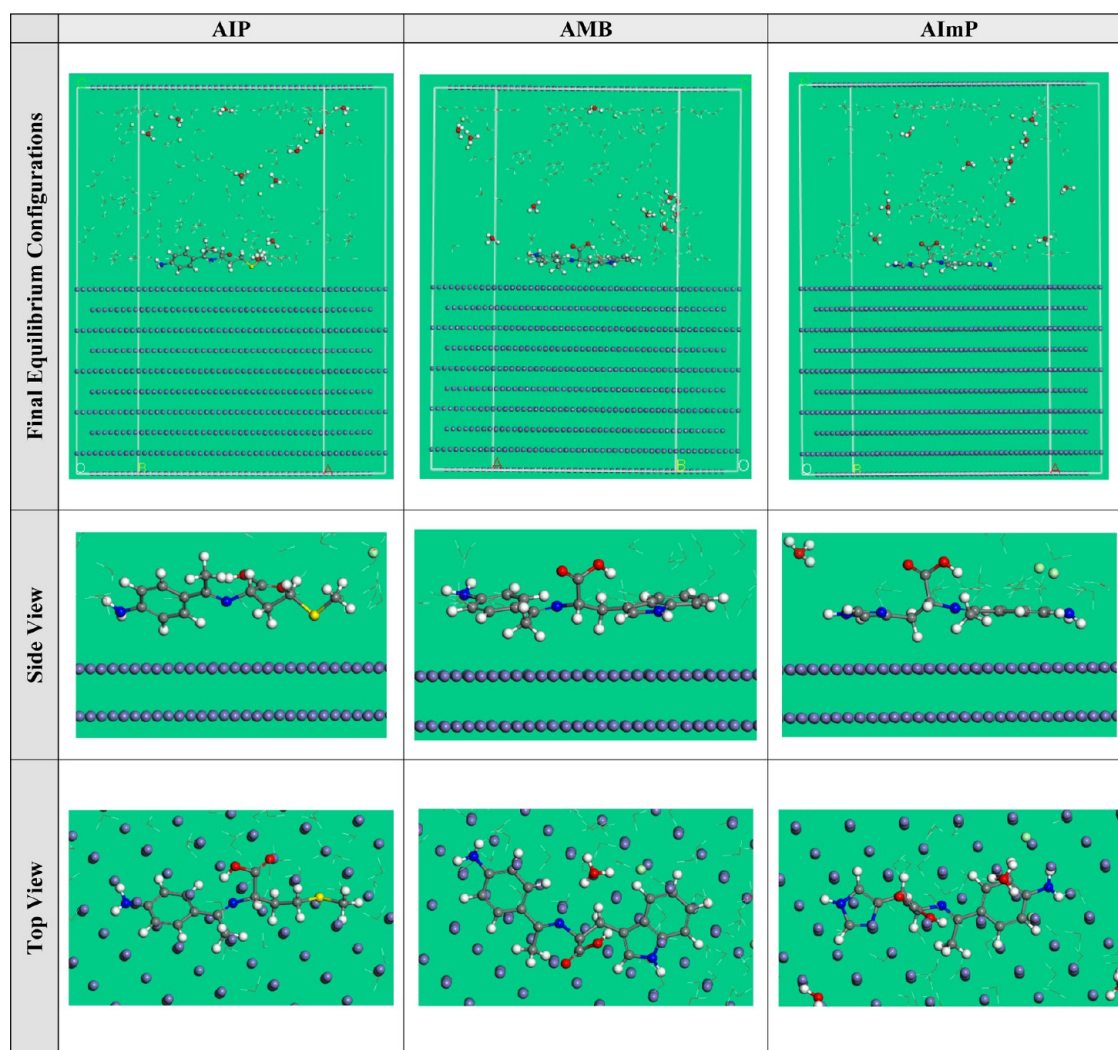


Figure 16. Highest proper adsorption arrangement for the investigated compounds AIP, AMB, and AImP on Fe(110) accomplished using an adsorption locator module.

Table 4. Data and Descriptors Calculated Using MC Simulations for the Adsorption of the Investigated Compounds AIP, AMB, and AImP on Fe(110)

corrosion systems	adsorption energy (kcal mol ⁻¹)	rigid adsorption energy (kcal mol ⁻¹)	deformation energy (kcal mol ⁻¹)	dE_{ads}/dN_i ; inhibitor (kcal mol ⁻¹)	dE_{ads}/dN_i ; Cl ⁻ ions (kcal mol ⁻¹)	dE_{ads}/dN_i ; hydronium (kcal mol ⁻¹)	dE_{ads}/dN_i ; water (kcal mol ⁻¹)
Fe(110) AIP water hydronium Cl ⁻ ions	-3212.23	-3035.63	-176.60	-284.47	-105.62	-63.64	-15.18
Fe(110) AMB water hydronium Cl ⁻ ions	-3286.05	-3100.53	-185.52	-306.61	-106.86	-65.42	-15.68
Fe(110) AImP water hydronium Cl ⁻ ions	-3174.46	-3005.09	-169.37	-261.27	-104.12	-64.06	-15.41

dissolution) and cathodic process (hydrogen evolution or oxygen reduction).⁵⁷ The main important role of employing the

organic inhibitors is to suppress the oxidation of the metallic surface and prevent oxygen and water from diffusing onto the

Table 5. Comparing the Inhibition Efficiency of Recently Published Schiff Bases as Corrosion Inhibitors with Those of the Investigated Schiff Bases Used in This Study

inhibitor code	steel alloy	corrosive medium	optimum concentration	maximum inhibition %	reference
PAMP	mild steel	1.0 M HCl	800 ppm	87.2	61
PPM				92.9	
OQ	mild steel	1.0 M HCl	5.0×10^{-3} M	93.8	62
EQ				92.7	
MQ				91.8	
PMTTA	mild steel	1.0 M HCl	175 ppm	92.7	20
PATT				91.1	
PMTA				87.8	
PTA				80.5	
CBTA	mild steel	1.0 M HCl	6 ppm	82.4	63
PATA				90.4	
MBTA				92.8	
MTMP				96.7	
IICH	mild steel	1.0 M HCl	200 ppm	97.9	14
ICCH				95.3	
IBCH				92.2	
IMCH				99.3	
L400	carbon steel	1.0 M HCl	1×10^{-4} M	92.0	64
L600				94.0	
Cpd I	carbon steel	1.0 M HCl	250 ppm	77.9	65
Cpd II				81.1	
Cpd III				85.4	
S1	carbon steel	1.0 M HCl	100 ppm	89.5	66
S2				91.8	
azoS8	carbon steel	1.0 M HCl	500 ppm	91.3	67
BTTM	mild steel	1.0 M H ₂ SO ₄	10.2×10^{-4} M	95.6	68
Chi-Cn1	mild steel	0.5 M H ₂ SO ₄	350 ppm	83.1	69
Chi-Cn2				90.3	
Chi-Cn3				92.6	
Chi-Cn4				93.6	
Chi-Cn5				96.2	
INB	carbon steel	0.5 M H ₂ SO ₄	1.0×10^{-3} M	90.2	70
IMB				91.5	
AIP	carbon steel	1.0 M HCl	10 mM	93.2	this work
AMP				96.01	
AImp				77.03	

metal surface, and this will be achieved by the adoption of the inhibitors on the metallic surface.⁵⁸ The anticipated corrosion protection mechanism of the explored Schiff bases for Q235 steel in HCl solution in this study could be proposed as follows.

In a corrosive acidic medium, the steel surface will be positively charged due to metallic oxidation. Moreover, the negatively charged chloride ions of HCl will be attracted to the positively charged steel surface, promoting the metal dissolution. The heteroatoms of the explored inhibitor molecules in acidic media are protonated, which makes it easy to attract to the oppositely charged counterions via electrostatic force and adsorbed on the metallic surface.⁵⁹ After adsorption, the explored inhibitors can return to their neutral forms and then move their nonbonding electrons to d-orbitals of steel via a coordination bond through the chemisorption process. Consequently, the adsorption process of these compounds on the steel surface involved both physical and chemical adsorption processes.⁶⁰ The investigated inhibitors contain various heteroatoms such as oxygen, nitrogen, and sulfur, which can donate lone pairs of electrons to empty d-orbitals of the iron of steel, facilitating their adsorption. Furthermore, the presence of an aromatic ring, indole, and imidazole groups can be oriented

toward the cathodic sites and facilitate the formation of an adsorbed layer that serves as a barrier among the alloy surface and corrosive solution. The presence of both neutral and protonated C and N elements in the interfacial film on the steel surface implies that the adsorbed constituents of **AMB** involved both protonated and nonprotonated (molecular) species. This would involve the electrostatic interaction of protonated species and the charged Fe surface (physisorption), possibly mediated by adsorbed anions (Cl⁻), as well as covalent interactions between the unprotonated heteroatoms and vacant d-orbitals of Fe (chemisorption). The different characterization techniques like XPS, SEM, EDS, FTIR, and UV–vis approve the adsorption of the examined organic compounds on the steel surface, which is responsible for the pronounced surface protection compared with the bare steel surface, with the best protection recorded in the existence of the **ABM** inhibitor owing to the formation of a protecting film on the steel surface, which hinders the steel dissolution and penetration of the corrosive ions to the surface.

3.12. Assessing the Inhibition Efficiency of the Investigated Schiff Base Derivatives. The inhibition efficiency of the examined Schiff base was compared to that of the other published Schiff bases, as depicted in **Table 5**. Based on

the results presented in this table, the investigated newly designed Schiff bases demonstrated superior corrosion inhibition performance compared to previously reported Schiff bases as inhibitors for Q235 steel alloy in an acidic HCl solution. The outstanding outcomes of this study imply that the newly designed Schiff bases possess unique structural elements and/or functional groups that play a part in their improved ability to inhibit corrosion. These characteristics could include aromatic rings, electron-donating groups, or other chemical moieties that are known to support corrosion inhibition.

4. CONCLUSIONS

In the present study, the newly synthesized compounds (AIP, AMB, and AImP) significantly protect Q235 steel from corrosion in an acidic solution (1.0 M HCl) and the investigation eventually results in the following conclusions:

- PDP and EIS results indicated the inhibition efficacy of the investigated inhibitors, which increases with increasing the inhibitor concentration.
- The PDP measurements designate that the examined inhibitors exhibit features of mixed-type inhibitors with high protection efficiencies of 93.15, 96.01, and 77.03% in the presence of AIP, AMB, and AImP, respectively.
- EIS measurements confirm the formation of an adsorbed protective layer via decreasing in C_{dl} values and increasing in R_{ct} values.
- The surface analysis (SEM and EDS) as well as XPS, UV–vis, and FTIR confirmed the inhibiting film formed on the steel surface by the examined inhibitors, with significant inhibition recorded in the case of AMB.
- Mechanism of the inhibition was investigated theoretically using the DFT calculations and MC simulations, which validated the experimental findings and confirmed that the adsorption of the examined inhibitor molecules on the steel surface occurs via active sites like $-O$, $-N$, and $-S$ atoms and the π -bonds of the aromatic rings.
- The results recorded from the electrochemical, theoretical, and surface analyses are consistent.

■ AUTHOR INFORMATION

Corresponding Authors

Qahtan A. Yousif – Department of Materials Engineering, College of Engineering, University of Al-Qadisiyah, Al Diwaniyah 111111, Iraq; Email: qahtan.adnan@qu.edu.iq
Ahmed Abdel Nazeer – Nanotechnology and Advanced Materials Program, Energy & Building Research Center, Kuwait Institute for Scientific Research (KISR), Safat 13109, Kuwait; Electrochemistry Laboratory, Physical Chemistry Department, National Research Center, Giza 12622, Egypt; orcid.org/0000-0003-3886-1511; Email: aanazeer@kISR.edu.kw

Authors

Zainb Fadel – General Directorate of Education Al-Qadisiyah, Ministry of Education, Al-Qadisiyah 001, Iraq
Latifa A. Al-Hajji – Nanotechnology and Advanced Materials Program, Energy & Building Research Center, Kuwait Institute for Scientific Research (KISR), Safat 13109, Kuwait
Kamal Shalabi – Department of Chemistry, College of Science and Humanities in Al-Kharj, Prince Sattam bin Abdulaziz University, Al-Kharj 11942, Saudi Arabia; Chemistry Department, Faculty of Science, Mansoura University,

Mansoura 35516, Egypt; orcid.org/0000-0001-5478-6369

Complete contact information is available at:
<https://pubs.acs.org/10.1021/acsomega.3c09688>

Notes

The authors declare no competing financial interest.

■ REFERENCES

- (1) Abdelsalam, M. M.; Bedair, M. A.; Hassan, A. M.; et al. Green synthesis, electrochemical, and DFT studies on the corrosion inhibition of steel by some novel triazole Schiff base derivatives in hydrochloric acid solution. *Arabian J. Chem.* **2022**, *15* (1), No. 103491.
- (2) Majeed, M. N.; Yousif, Q. A.; Bedair, M. A. Study of the Corrosion of Nickel–Chromium Alloy in an Acidic Solution Protected by Nickel Nanoparticles. *ACS Omega* **2022**, *7* (34), 29850–29857.
- (3) Kesari, P.; Udayabhanu, G. Investigation of Vitamin B12 as a corrosion inhibitor for mild steel in HCl solution through gravimetric and electrochemical studies. *Ain Shams Eng. J.* **2023**, *14* (4), No. 101920.
- (4) Fernine, Y.; Salim, R.; Arrousse, N.; et al. Anti-corrosion performance of Ocimum basilicum seed extract as environmental friendly inhibitors for mild steel in HCl solution: Evaluations of electrochemical, EDX, DFT and Monte Carlo. *J. Mol. Liq.* **2022**, *355*, No. 118867.
- (5) Abd El-Lateef, H. M.; Khalaf, M. M.; Gouda, M.; et al. Novel water-soluble organoselenocyanates and symmetrical diselenides tethered N-succinilate and N-maleanilate as corrosion inhibitors for reinforced steel in the simulated concrete pore solution. *Constr. Build. Mater.* **2023**, *366*, No. 130135.
- (6) Yousif, Q. A.; Majeed, M. N.; Bedair, M. A. Surface protection against corrosion of Ni turbine blades by electrophoretic deposition of MnO_2 , TiO_2 and $TiO_2 - C$ nanocoating. *RSC Adv.* **2022**, *12* (52), 33725–33736.
- (7) Williams, G.; Coleman, A. J.; McMurray, H. N. Inhibition of Aluminium Alloy AA2024-T3 pitting corrosion by copper complexing compounds. *Electrochim. Acta* **2010**, *55* (20), 5947–5958.
- (8) Yousif, Q. A.; Fadel, Z.; Abuelela, A. M.; Alosaimi, E. H.; Melhi, S.; Bedair, M. A. Insight into the corrosion mitigation performance of three novel benzimidazole derivatives of amino acids for carbon steel (X56) in 1 M HCl solution. *RSC Adv.* **2023**, *13* (19), 13094–13119.
- (9) Shafek, S. H.; Ghiaty, E. A.; El Basiony, N. M.; Badr, E. A.; Shaban, S. M. Preparation of zwitterionic ionic surfactants-based sulphonyl for steel protections: Experimental and theoretical insights. *Z. Phys. Chem.* **2023**, *237* (1–2), 1–33.
- (10) Alharthi, N. H.; El-Hashemy, M. A.; Derafa, W. M.; Althobaiti, I. O.; Altaieb, H. A. Corrosion inhibition of mild steel by highly stable polydentate schiff base derived from 1,3- propanediamine in aqueous acidic solution. *J. Saudi Chem. Soc.* **2022**, *26* (4), No. 101501.
- (11) Betti, N.; Al-Amiery, A. A.; Al-Azzawi, W. K.; Isahak, W. N. R. W. Corrosion inhibition properties of schiff base derivative against mild steel in HCl environment complemented with DFT investigations. *Sci. Rep.* **2023**, *13* (1), No. 8979.
- (12) Benmahammed, I.; Douadi, T.; Issaadi, S.; Al-Noaimi, M.; Chafaa, S. Heterocyclic Schiff bases as corrosion inhibitors for carbon steel in 1 M HCl solution: hydrodynamic and synergetic effect. *J. Dispersion Sci. Technol.* **2020**, *41* (7), 1002–1021.
- (13) Madani, A.; Kaabi, I.; Sibous, L.; Bentouhami, E. Synthesis, characterization and evaluation of the corrosion inhibition on mild steel of two new Schiff bases derived from 4,4'-diaminobiphenyl: Density functional theory investigation. *J. Iran. Chem. Soc.* **2021**, *18* (11), 3077–3095.
- (14) Singh, A. K.; Pandey, A. K.; Banerjee, P.; et al. Eco-friendly disposal of expired anti-tuberculosis drug isoniazid and its role in the protection of metal. *J. Environ. Chem. Eng.* **2019**, *7* (2), No. 102971.
- (15) Mustafa, A. M.; Sayyid, F.; Betti, N.; et al. Inhibition of mild steel corrosion in hydrochloric acid environment by 1-amino-2-mercapto-5-

- (4-(pyrrol-1-yl)phenyl)-1,3,4-triazole. *S. Afr. J. Chem. Eng.* **2022**, *39*, 42–51.
- (16) Feng, L.; Yang, H.; Wang, F. Experimental and theoretical studies for corrosion inhibition of carbon steel by imidazoline derivative in 5% NaCl saturated Ca(OH)₂ solution. *Electrochim. Acta* **2011**, *58*, 427–436.
- (17) Cruz, J.; Martínez-Aguilera, L. M. R.; Salcedo, R.; Castro, M. Reactivity properties of derivatives of 2-imidazoline: an ab initio DFT study. *Int. J. Quantum Chem.* **2001**, *85* (4–5), 546–556.
- (18) Yousif, Q. A. Environmentally sustainable disposal of expired albendazole medication and its role in the protection of mild steel. *IOP Conf. Ser.: Earth Environ. Sci.* **2021**, *790* (1), No. 012072.
- (19) Al-Amiery, A.; Salman, T. A.; Alazawi, K. F.; Shaker, L. M.; Kadhum, A. A. H.; Takriff, M. S. Quantum chemical elucidation on corrosion inhibition efficiency of Schiff base: DFT investigations supported by weight loss and SEM techniques. *Int. J. Low-Carbon Technol.* **2020**, *15* (2), 202.
- (20) Chugh, B.; Singh, A. K.; Thakur, S.; et al. Comparative investigation of corrosion-mitigating behavior of thiadiazole-derived bis-schiff bases for mild steel in acid medium: experimental, theoretical, and surface study. *ACS Omega* **2020**, *5* (23), 13503–13520.
- (21) Gupta, S. K.; Mitra, R. K.; Yadav, M.; et al. Electrochemical, surface morphological and computational evaluation on carbonylhydrazide Schiff bases as corrosion inhibitor for mild steel in acidic medium. *Sci. Rep.* **2023**, *13* (1), No. 15108.
- (22) Ibeji, C. U.; Akintayo, D. C.; Oluwasola, H. O.; Akintemi, E. O.; Onwukwe, O. G.; Ezimome, O. M. Synthesis, experimental and computational studies on the anti-corrosion performance of substituted Schiff bases of 2-methoxybenzaldehyde for mild steel in HCl medium. *Sci. Rep.* **2023**, *13* (1), No. 3265.
- (23) Abd El-Lateef, H. M.; Sayed, A. R.; Shalabi, K. Synthesis and theoretical studies of novel conjugated polyazomethines and their application as efficient inhibitors for C1018 steel pickling corrosion behavior. *Surf. Interfaces* **2021**, *23*, No. 101037.
- (24) El-Lateef, H. M. A.; Abdallah, Z. A.; Ahmed, M. S. M. Solvent-free synthesis and corrosion inhibition performance of Ethyl 2-(1,2,3,6-tetrahydro-6-oxo-2-thioxopyrimidin-4-yl)ethanoate on carbon steel in pickling acids: Experimental, quantum chemical and Monte Carlo simulation studies. *J. Mol. Liq.* **2019**, *296*, No. 111800.
- (25) Dehghani, A.; Mostafatabar, A. H.; Bahlakeh, G.; Ramezanzadeh, B. A detailed study on the synergistic corrosion inhibition impact of the Quercetin molecules and trivalent europium salt on mild steel; electrochemical/surface studies, DFT modeling, and MC/MD computer simulation. *J. Mol. Liq.* **2020**, *316*, No. 113914.
- (26) Feng, Y.; Chen, S.; Guo, W.; Zhang, Y.; Liu, G. Inhibition of iron corrosion by 5,10,15,20-tetraphenylporphyrin and 5,10,15,20-tetra-(4-chlorophenyl)porphyrin adlayers in 0.5 M H₂SO₄ solutions. *J. Electroanal. Chem.* **2007**, *602* (1), 115–122.
- (27) Abd El-Lateef, H. M.; Shalabi, K.; Tantawy, A. H. Corrosion inhibition and adsorption features of novel bioactive cationic surfactants bearing benzenesulphonamide on C1018-steel under sweet conditions: Combined modeling and experimental approaches. *J. Mol. Liq.* **2020**, *320*, No. 114564.
- (28) Fouda, A. S.; Abdel Nazeer, A.; El behairy, W. T. Assessment of Begonia Extract as New Eco-friendly Inhibitor for Low-Carbon-Steel Corrosion in Acidic Environment. *J. Bio-Tribo-Corros.* **2018**, *4* (1), No. 7.
- (29) Hegazy, M. A.; Nazeer, A. A.; Shalabi, K. Electrochemical studies on the inhibition behavior of copper corrosion in pickling acid using quaternary ammonium salts. *J. Mol. Liq.* **2015**, *209*, 419–427.
- (30) Al-sawah, M.; Nazeer, A. A.; Salah, L.; Durmuş, M.; Makhseed, S. Novel azaphthalocyanines with efficient anti-corrosion capability: Effect of halogens and heavy metals. *J. Mol. Liq.* **2019**, *293*, No. 111545.
- (31) Kundu, S.; Thakur, S.; et al. A Review of Electrochemical Techniques for Corrosion Monitoring—Fundamentals and Research Updates. *Crit. Rev. Anal. Chem.* **2023**, 1–26.
- (32) Al-Rashed, O.; Nazeer, A. A. Ionic liquid-assisted production of hydrophobic nanocomposite coating for mild steel corrosion prevention in saline medium. *J. Mater. Res. Technol.* **2022**, *18*, 5087–5102.
- (33) Boubour, E.; Lennox, R. B. Stability of ω -Functionalized Self-Assembled Monolayers as a Function of Applied Potential. *Langmuir* **2000**, *16* (19), 7464–7470.
- (34) Nazeer, A. A.; Al-Hetlani, E.; Amin, M. O.; Quiñones-Ruiz, T.; Lednev, I. K. A poly(butyl methacrylate)/graphene oxide/TiO₂ nanocomposite coating with superior corrosion protection for AZ31 alloy in chloride solution. *Chem. Eng. J.* **2019**, *361*, 485–498.
- (35) Wang, X.; Yang, H.; Wang, F. An investigation of benzimidazole derivative as corrosion inhibitor for mild steel in different concentration HCl solutions. *Corros. Sci.* **2011**, *53* (1), 113–121.
- (36) Husain, E.; Abdel Nazeer, A.; Alsarraf, J.; et al. Corrosion behavior of AISI 316 stainless steel coated with modified fluoropolymer in marine condition. *J. Coat. Technol. Res.* **2018**, *15* (5), 945–955.
- (37) Haldhar, R.; Prasad, D.; Bhardwaj, N. Extraction and experimental studies of *Citrus aurantifolia* as an economical and green corrosion inhibitor for mild steel in acidic media. *J. Adhes. Sci. Technol.* **2019**, *33* (11), 1169–1183.
- (38) El Faydy, M.; Lakhrissi, B.; Guenbour, A.; et al. In situ synthesis, electrochemical, surface morphological, UV-visible, DFT and Monte Carlo simulations of novel 5-substituted-8-hydroxyquinoline for corrosion protection of carbon steel in a hydrochloric acid solution. *J. Mol. Liq.* **2019**, *280*, 341–359.
- (39) Tourabi, M.; Nohair, K.; Traisnel, M.; Jama, C.; Bentiss, F. Electrochemical and XPS studies of the corrosion inhibition of carbon steel in hydrochloric acid pickling solutions by 3, 5-bis (2-thienylmethyl)-4-amino-1, 2, 4-triazole. *Corros. Sci.* **2013**, *75*, 123–133.
- (40) Han, P.; Chen, C.; Li, W.; et al. Synergistic effect of mixing cationic and nonionic surfactants on corrosion inhibition of mild steel in HCl: experimental and theoretical investigations. *J. Colloid Interface Sci.* **2018**, *516*, 398–406.
- (41) Njoku, D. I.; Njoku, C. N.; Lgaz, H.; Okafor, P. C.; Oguzie, E. E.; Li, Y. Corrosion protection of Q235 steel in acidic-chloride media using seed extracts of Piper guineense. *J. Mol. Liq.* **2021**, *330*, No. 115619.
- (42) Wang, Y.; Qiang, Y.; Zhi, H.; Ran, B.; Zhang, D. Evaluating the synergistic effect of maple leaves extract and iodide ions on corrosion inhibition of Q235 steel in H₂SO₄ solution. *J. Ind. Eng. Chem.* **2023**, *117*, 422–433.
- (43) Qiang, Y.; Guo, L.; Li, H.; Lan, X. Fabrication of environmentally friendly Losartan potassium film for corrosion inhibition of mild steel in HCl medium. *Chem. Eng. J.* **2021**, *406*, No. 126863.
- (44) Palaniappan, N.; Cole, I. S.; Kuznetsov, A. E. Experimental and computational studies of graphene oxide covalently functionalized by octylamine: electrochemical stability, hydrogen evolution, and corrosion inhibition of the AZ13 Mg alloy in 3.5% NaCl. *RSC Adv.* **2020**, *10* (19), 11426–11434.
- (45) Lukovits, I.; Kálmán, E.; Zucchi, F. Corrosion Inhibitors—Correlation between Electronic Structure and Efficiency. *CORROSION* **2001**, *57* (1), 3–8.
- (46) Yesudass, S.; Olasunkanmi, L.; Bahadur, I.; Kabanda, M. M.; Obot, I. B.; Ebenso, E. Experimental and theoretical studies on some selected ionic liquids with different cations/anions as corrosion inhibitors for mild steel in acidic medium. *J. Taiwan Inst. Chem. Eng.* **2016**, *64*, 252–268.
- (47) Debab, H.; Douadi, T.; Daoud, D.; Issaadi, S.; Chafaa, S. Electrochemical and quantum chemical studies of adsorption and corrosion inhibition of two new schiff bases on carbon steel in hydrochloric acid media. *Int. J. Electrochem. Sci.* **2018**, *13* (7), 6958–6977.
- (48) Gao, G.; Liang, C. Electrochemical and DFT studies of β -amino-alcohols as corrosion inhibitors for brass. *Electrochim. Acta* **2007**, *52* (13), 4554–4559.
- (49) Abd El-Lateef, H. M.; Shalabi, K.; Tantawy, A. H. Corrosion inhibition of carbon steel in hydrochloric acid solution using newly synthesized urea-based cationic fluorosurfactants: experimental and computational investigations. *New J. Chem.* **2020**, *44*, 17791.
- (50) Goyal, M.; Vashist, H.; Kumar, S.; Bahadur, I.; Benhiba, F.; Zarrouk, A. Acid corrosion inhibition of ferrous and non-ferrous metal

by nature friendly Ethoxycarbonylmethyltriphenylphosphonium Bromide (ECMTPB): Experimental and MD simulation evaluation. *J. Mol. Liq.* **2020**, *315*, No. 113705.

(51) Oyebamiji, A. K.; Adeleke, B. B. Quantum chemical studies on inhibition activities of 2,3-dihydroxypropyl-sulfanyl derivative on carbon steel in acidic media. *Int. J. Corros. Scale Inhib.* **2018**, *7* (4), 498–508.

(52) Gece, G.; Bilgiç, S. Quantum chemical study of some cyclic nitrogen compounds as corrosion inhibitors of steel in NaCl media. *Corros. Sci.* **2009**, *51* (8), 1876–1878.

(53) Madkour, L. H.; Kaya, S.; Obot, I. B. Computational, Monte Carlo simulation and experimental studies of some arylazotriazoles (AATR) and their copper complexes in corrosion inhibition process. *J. Mol. Liq.* **2018**, *260*, 351–374.

(54) Shalabi, K.; Helmy, A. M.; El-Askalany, A. H.; Shahba, M. M. New pyridinium bromide mono-cationic surfactant as corrosion inhibitor for carbon steel during chemical cleaning: Experimental and theoretical studies. *J. Mol. Liq.* **2019**, *293*, No. 111480.

(55) Özcan, M.; Dehri, I.; Erbil, M. Organic sulphur-containing compounds as corrosion inhibitors for mild steel in acidic media: correlation between inhibition efficiency and chemical structure. *Appl. Surf. Sci.* **2004**, *236* (1–4), 155–164.

(56) Dehghani, A.; Mostafatabar, A. H.; Bahlakeh, G.; Ramezanzadeh, B. A detailed study on the synergistic corrosion inhibition impact of the Quercetin molecules and trivalent europium salt on mild steel; electrochemical/surface studies, DFT modeling, and MC/MD computer simulation. *J. Mol. Liq.* **2020**, *316*, No. 113914.

(57) Abdel Nazeer, A.; El-Abbasy, H. M.; Fouda, A. S. Adsorption and Corrosion Inhibition Behavior of Carbon Steel by Cefoperazone as Eco-Friendly Inhibitor in HCl. *J. Mater. Eng. Perform.* **2013**, *22* (8), 2314–2322.

(58) Mandour, H. S.; Nazeer, A. A.; Al-Hetlani, E.; Madkour, M.; Abdel-Monem, Y. K. Organic nanoparticles of acetohydrazides as novel inhibitors for mild steel corrosion. *New J. Chem.* **2018**, *42* (8), 5914–5922.

(59) Al-Rashed, O. A.; Nazeer, A. A. Ionic liquids with superior protection for mild steel in acidic media: Effects of anion, cation, and alkyl chain length. *J. Mol. Liq.* **2019**, *288*, No. 111015.

(60) Azeez, F. A.; Al-Rashed, O. A.; Nazeer, A. A. Controlling of mild-steel corrosion in acidic solution using environmentally friendly ionic liquid inhibitors: Effect of alkyl chain. *J. Mol. Liq.* **2018**, *265*, 654–663.

(61) Li, X.; Chen, L.; Xie, B.; et al. Two semi flexible nonplanar double Schiff bases as corrosion inhibitors for mild steel in HCl solution: Experimental and theoretical investigations. *J. Environ. Chem. Eng.* **2023**, *11* (3), No. 110077.

(62) Hamani, H.; Daoud, D.; Benabid, S.; Douadi, T. Electrochemical, density functional theory (DFT) and molecular dynamic (MD) simulations studies of synthesized three news Schiff bases as corrosion inhibitors on mild steel in the acidic environment. *J. Indian Chem. Soc.* **2022**, *99* (7), No. 100492.

(63) Singh, A. K.; Chugh, B.; Thakur, S.; et al. Green approach of synthesis of thiazolyl imines and their impeding behavior against corrosion of mild steel in acid medium. *Colloids Surf., A* **2020**, *599*, No. 124824.

(64) Bedir, A. G.; Abd El-raouf, M.; Abdel-Mawgoud, S.; Negm, N. A.; El Basiony, N. M. Corrosion inhibition of carbon steel in hydrochloric acid solution using ethoxylated nonionic surfactants based on schiff base: electrochemical and computational investigations. *ACS Omega* **2021**, *6* (6), 4300–4312.

(65) Thabet, H. K.; AlGhamdi, J. M.; Mohammed, H. A.; Elsaïd, M. A. M.; Ashmawy, A. M. Anticorrosion Agents for Carbon Steel in Acidic Environments: Synthesis and Quantum Chemical Analysis of New Schiff Base Compounds with Benzylidene. *ACS Omega* **2023**, *8* (42), 39770–39782.

(66) Altalhi, A. A. Anticorrosion investigation of new diazene-based Schiff base derivatives as safe corrosion inhibitors for API X65 steel pipelines in acidic oilfield formation water: synthesis, experimental, and computational studies. *ACS Omega* **2023**, *8* (34), 31271–31280.

(67) Alanazi, K. D.; Alshammari, B. H.; Alanazi, T. Y. A.; et al. Green Synthesis of a Novel Cationic Surfactant Based on an Azo Schiff Compound for Use as a Carbon Steel Anticorrosion Agent. *ACS Omega* **2023**, *8*, 49009.

(68) Singh, A. K.; Singh, M.; Thakur, S.; et al. Adsorption study of N (-benzo [d] thiazol-2-yl)-1-(thiophene-2-yl) methanimine at mild steel/aqueous H₂SO₄ interface. *Surf. Interfaces* **2022**, *33*, No. 102169.

(69) Chugh, B.; Singh, A. K.; Poddar, D.; Thakur, S.; Pani, B.; Jain, P. Relation of degree of substitution and metal protecting ability of cinnamaldehyde modified chitosan. *Carbohydr. Polym.* **2020**, *234*, No. 115945.

(70) Al-Sharif, M. S. Electrochemical and Theoretical Assessment of Two Heterocyclic Schiff Bases as Effective Corrosion Inhibitors for Carbon Steel in Sulfuric Acid Solution. *Int. J. Electrochem. Sci.* **2024**, *19*, No. 100454.